NBS SPECIAL PUBLICATION 400-49

U.S. DEPARTMENT OF COMMERCE / National Bureau of Standards

*Semiconductor Measurement Technology:*

# Angular Sensitivity of Controlled Implanted Doping Profiles

## NATIONAL BUREAU OF STANDARDS

The National Bureau of Standards[1] was established by an act of Congress March 3, 1901. The Bureau's overall goal is to strengthen and advance the Nation's science and technology and facilitate their effective application for public benefit. To this end, the Bureau conducts research and provides: (1) a basis for the Nation's physical measurement system, (2) scientific and technological services for industry and government, (3) a technical basis for equity in trade, and (4) technical services to promote public safety. The Bureau's technical work is performed by the National Measurement Laboratory, the National Engineering Laboratory, and the Institute for Computer Sciences and Technology.

**THE NATIONAL MEASUREMENT LABORATORY** provides the national system of physical and chemical and materials measurement; coordinates the system with measurement systems of other nations and furnishes essential services leading to accurate and uniform physical and chemical measurement throughout the Nation's scientific community, industry, and commerce; conducts materials research leading to improved methods of measurement, standards, and data on the properties of materials needed by industry, commerce, educational institutions, and Government; provides advisory and research services to other Government Agencies; develops, produces, and distributes Standard Reference Materials; and provides calibration services. The Laboratory consists of the following centers:

Absolute Physical Quantities[2] — Radiation Research — Thermodynamics and Molecular Science — Analytical Chemistry — Materials Science.

**THE NATIONAL ENGINEERING LABORATORY** provides technology and technical services to users in the public and private sectors to address national needs and to solve national problems in the public interest; conducts research in engineering and applied science in support of objectives in these efforts; builds and maintains competence in the necessary disciplines required to carry out this research and technical service; develops engineering data and measurement capabilities; provides engineering measurement traceability services; develops test methods and proposes engineering standards and code changes; develops and proposes new engineering practices; and develops and improves mechanisms to transfer results of its research to the utlimate user. The Laboratory consists of the following centers:

Applied Mathematics — Electronics and Electrical Engineering[2] — Mechanical Engineering and Process Technology[2] — Building Technology — Fire Research — Consumer Product Technology — Field Methods.

**THE INSTITUTE FOR COMPUTER SCIENCES AND TECHNOLOGY** conducts research and provides scientific and technical services to aid Federal Agencies in the selection, acquisition, application, and use of computer technology to improve effectiveness and economy in Government operations in accordance with Public Law 89-306 (40 U.S.C. 759), relevant Executive Orders, and other directives; carries out this mission by managing the Federal Information Processing Standards Program, developing Federal ADP standards guidelines, and managing Federal participation in ADP voluntary standardization activities; provides scientific and technological advisory services and assistance to Federal Agencies; and provides the technical foundation for computer-related policies of the Federal Government. The Institute consists of the following divisions:

Systems and Software — Computer Systems Engineering — Information Technology.

[1]Headquarters and Laboratories at Gaithersburg, Maryland, unless otherwise noted; mailing address Washington,D.C. 20234.
[2]Some divisions within the center are located at Boulder, Colorado, 80303.

**The National Bureau of Standards was reorganized, effective April 9, 1978.**

*Semiconductor Measurement Technology:*

# Angular Sensitivity of Controlled Implanted Doping Profiles

Robert G. Wilson, Howard L. Dunlap, and
Douglas M. Jamba

Hughes Research Laboratories
3011 Malibu Canyon Road
Malibu, CA 90265

and

David R. Myers

Electron Devices Division
Center for Electronics & Electrical Engineering
National Engineering Laboratory
National Bureau of Standards
Washington, D.C. 20234

Jointly supported by:

The Defense Advanced Research Projects Agency

and

The National Bureau of Standards


U.S. DEPARTMENT OF COMMERCE, Juanita M. Kreps, Secretary

Dr. Sidney Harman, Under Secretary

Jordan J. Baruch, Assistant Secretary for Science and Technology

NATIONAL BUREAU OF STANDARDS, Ernest Ambler, Director

Issued November 1978

**Library of Congress Cataloging in Publication Data**

Main entry under title:

Angular sensitivity of controlled implanted doping profiles.

(Semiconductor measurement technology) (NBS special publications ; 400-49)

Supt. of Doc. no.: C 13.10:400-49

1. Semiconductor doping. 2. Ion implantation. 3. Integrated circuits. I. Wilson, Robert G. II. Series. III. Series: United States. National Bureau of Standards. Special publication ; 400-49.

QC100.U57 no. 400-49 [TK7871.85] 602'.1s 78-10624

[621.3815'2'028]

National Bureau of Standards Special Publication 400-49

Nat. Bur. Stand. (U.S.), Spec. Publ. 400-49, 61 pages (Nov. 1978)

CODEN: XNBSAV

U.S. GOVERNMENT PRINTING OFFICE

WASHINGTON: 1978

For sale by the Superintendent of Documents, U.S. Government Printing Office, Washington, D.C. 20402

Stock No. 003-003-01997-6 Price $2.50

(Add 25 percent additional for other than U.S. mailing).

CONTENTS



LIST OF FIGURES

PAGE

# PREFACE

This study was carried out at the Hughes Research Laboratories as a part of the Semiconductor Technology Program in the Electron Devices Division at the National Bureau of Standards. The Semiconductor Technology Program serves to focus NBS research to enhance the performance, interchangeability, and reliability of discrete semiconductor devices and integrated circuits through improvements in measurement technology for use in specifying materials and devices in national and international commerce and for use by industry in controlling device fabrication processes. The Hughes portions of this work were supported by the Defense Advanced Research Projects Agency, ARPA Order 2397, Program Code 6D10, through the National Bureau of Standards Semiconductor Technology Program, Contract 5-35891. The contract was monitored by Richard L. Raybold as the Contracting Officer's Technical Representative. Drs. W. M. Bullis and K. F. Galloway provided technical review of this report for the National Bureau of Standards.

The authors wish to thank Dr. C. L. Anderson for his thorough reading of the manuscript and many constructive suggestions, acknowledge A. J. Mohr and R. R. Hart for designing and building the precision target goniometer, and wish to thank Dr. J. Comas and H. B. Dietrich of the Naval Research Laboratories for providing the SIMS measurements and for useful discussions, respectively.

During the conduct of this work, D. R. Myers received support from an NBS-NRC postdoctoral fellowship.

# Angular Sensitivity of Controlled Implanted Doping Profiles

by

Robert G. Wilson, Howard L. Dunlap, Douglas M. Jamba,
and David R. Myers

*Abstract:* Ion implantation can be used to produce accurately controlled doping profiles for silicon devices and integrated circuits. The work reported here determines the angle at which the ion beam must strike the substrate in order to maintain control over the channeled and random equivalent depth distributions of carriers as measured by 1-MHz differential capacitance-voltage (C-V) profiling. A method to calculate the classical critical angle for channeling ($\psi_c$) is presented. Data are presented that characterize the variation in the depth distribution of carriers with substrate orientation, incident ion species, and incident ion energy, for a range of critical angles. This study establishes the degree of control of the angle between the ion beam and the crystallographic orientation needed to produce the limiting cases of either optimal channeling or maximum randomization of ion trajectory in the substrate. For the cases studied here, the angle between the ion beam and the substrate orientation must be controlled to within 0.5 ± 0.2 deg to obtain the optimally channeled depth distribution for implantation directly into the low index crystallographic orientations. Alternatively, to minimize unintentional channeling, the substrate must be oriented so that the nearest low index crystallographic direction is at least twice the classical critical angle away from the beam direction. The substrate tilt angles required to satisfy these conditions can exceed the 7- to 10-deg tilt commonly used in ion implantation. The implications of these results for uniform and reproducible ion implantation within the semiconductor industry are discussed.

*Key Words:* C-V profiling; controlled doping profiles; critical channeling angle; ion beam scanning; ion channeling; ion implantation; Rutherford backscattering alignment; silicon crystallographic orientation.

## 1. INTRODUCTION AND SUMMARY

This report presents the results of a study to determine how control of carrier depth distributions resulting from ion implantation into single

crystal silicon depends on the angle of incidence between the ion beam and the substrate crystallographic orientation. It is well known that ion range distributions in single crystal targets can be affected by ion channeling, the phenomenon in which ions are steered down the axial lattice channels by correlated collisions with the ordered arrangement of the substrate atoms. This effect leads to increased penetration depths for the ions that channel and also reduces the amount of radiation damage caused by the ion beam. With the present emphasis on shallower active regions in semiconductor devices, the extent of ion channeling should be minimized to reduce the formation of deeply penetrating tails in the dopant distribution, thereby leading to more predictable dopant profiles. Alternatively, when ion channeling is intentionally employed as a doping technique (for example, to create buried layers), it is important to be able to estimate how well the beam must be collimated and oriented to the crystal direction to obtain the optimally channeled distribution. Unlike most previous studies of ion channeling, the present work considers a range of atomic number ($Z_1$) and energy ($E_1$) representative of most laboratory implantation today. This work presents experimental data that demonstrate the change in the distribution of carriers with substrate orientation, incident ion species, and ion energy. The data empirically establish the control needed to guarantee a particular quality of channeled implanted carrier depth distribution and demonstrate that the implantation angle must be controlled to within 0.5 ± 0.2 deg to retain the optimally channeled distribution. A simple procedure is developed to calculate the classical critical angle for ion channeling ($\psi_c$), which is then correlated with the experimental data. Both the theory and the data clearly indicate that to minimize unintentional channeling during implantation, the wafer must be tilted so that the nearest low index crystal direction is at an angle to the beam direction of at least twice the critical angle. The present work thus demonstrates that the angle required to minimize unintentional channeling can under some conditions exceed the 7- to 10-deg tilt commonly used in implantation to simulate or achieve the "random equivalent" condition.

The experimental technique used in this investigation was to implant ions at various angles away from accurately channeled alignment and toward the direction of random equivalent (RE) orientation up to the random equivalent angle of about 7 deg, and to record the changes in depth distribution of carriers measured by differential capacitance-voltage (C-V) profiling. The implantation dose was usually $1.5 \times 10^{12}$ $cm^{-2}$, and the implants were annealed at 800°C for 20 or 30 min, which was found to fully activate all of these low fluence implants. The implantation angle was controlled to better than 0.1 deg for small angles (0.0 to 3.0 deg) away from axial alignment by the combination of Rutherford backscattering [1] and a target goniometer capable of controlling the angle to about 0.02 deg. The less sensitive angles from 3 to 7 deg were varied by tilting a standard target mount with the angle measured goemetrically. The ions studied were boron, arsenic, and indium at 300, 150, 75, 40, and 20 keV to fill in the range of critical angles from 2 to 7 deg. In order to provide a comparison between these C-V electrical profiles and corresponding atomic depth distributions, a set of profiles was measured for 150-

keV boron as a function of alignment away from the [110] axis of silicon using secondary ion mass spectroscopy (SIMS).

There are three previously reported investigations related to this study. One is a limited set of partial profiles reported by Seidel [2] for 150-keV boron in (111) silicon. Another is a set of profiles for phosphorus in (111) silicon, reported by Moline [3] and by Moline and Reutlinger [4]. A detailed set of profiles was reported by Reddi and Sansbury [5] for 450-keV phosphorus in the major lattice directions of silicon. These last data were analyzed and are included in the data compilation used in this report.

## 2. EXPERIMENTAL TECHNIQUES

### 2.1. Capacitance-Voltage Profiling

The depth distributions of acceptor or donor electrical activity were measured by the differential capacitance-voltage technique. This technique has been discussed by Moline [3], Seidel [2], and Reddi and Sansbury [5]; however, the present work uses reverse-biased Schottky barriers on implanted layers in ∿10- or 100-Ω·cm silicon substrates, rather than the $p$-$n$ junction or epilayer techniques. Acceptor impurities were implanted into $p$-type substrates, while donor impurities were implanted into $n$-type substrates. The C-V profiler used was an improved version of that described by Gordon, Stover, and Harp [6]. Contact was made to the back surface of the wafer by an annealed $10^{15}$ cm$^{-2}$ implant of boron (for $p$-type substrates) or arsenic (for $n$-type substrates). The implanted samples were annealed in nitrogen gas drawn from liquid nitrogen. Schottky barrier diodes of ∿0.13-mm diameter were formed by evaporation of ∿1000 Å of aluminum (on $p$-type silicon) or gold (on $n$-type silicon). The background level corresponding to the substrate doping was subtracted from the C-V profiles. The corrections to C-V profiles proposed by Kennedy, *et al.* [7] and by Moline [3], and calculated and illustrated by Reddi and Sansbury [5] and by Moline [3], had only a small effect on the profiles reported in this work. This correction has its greatest effect on the tail regions of the profiles. Although the correction affects only 0.1 to 1 percent of the implanted ions, this is sufficient to cause an apparent change of 1 to 10 percent in the magnitude of a channeling tail when 10 percent of the ions channel.

The effect of experimental factors on the C-V profiling equations for $n(x)$ and $x$ has been examined in terms of the sensitivity of the measurement system to the quality factor $[=(\omega C_S R_S)^{-1}]$ of the diodes studied, where $\omega$ is the angular measurement frequency, and $C_S$ and $R_S$ are, respectively, the capacitance and series resistance of the Schottky barrier diode (corrected to include spreading resistance). The results show that for the 0.13-mm diameter Schottky barriers with zero-bias capacitances of 1 to 15 pF and the 10- and 100-Ω·cm substrate resistances corrected for spreading resistances, the C-V profiles are accurate to 1 or 2 percent for $n(x) \leq 10^{17}$ cm$^{-3}$. For $C_S > 20$ pF, errors greater than 2 percent may begin to occur near $10^{17}$ cm$^{-3}$; however, the distributions for these con-

ditions are closer to the surface than 1000 Å and such data are not used or reported.

### 2.2. Silicon Crystal Alignment and Angular Control

Two techniques were used in this work to vary the implantation angle, one for angles from 0 to 3 deg with an accuracy of ∿0.02 deg and one for angles from 3 to 7 deg with an accuracy of ∿0.7 deg. Reduced accuracy was tolerable for the larger angles because of the lower sensitivity of implantation profile to angle in this range (near the random equivalent orientation).

Rutherford backscattering of light ions was used in combination with a precision target goniometer to align the silicon crystals for the low angle implantation.

The silicon crystals were accurately aligned at small angles by a technique similar to that originally described by Andersen, *et al.* [1], but with adjustments in crystal position so that the channeling axis was made collinear with the axis of rotation. This technique is based on the measurement of the decrease in backscattered proton (or alpha) yield as the major crystal planes are rotated through a highly collimated proton beam. The backscattered protons are detected by a surface barrier detector of 8- to 15-keV FWHM resolution located about 8 cm from the goniometer face, as illustrated in figure 1. Referring to figure 1, the backscattered proton yield as a function of azimuthal angle $\phi$ at a constant tilt angle of $\theta$ = 3.5 deg is shown in figure 2 for 140-keV protons incident on the (111) face of a silicon crystal. An energy discriminator is adjusted to permit only protons scattered near the surface to be counted. Distinct dips or decreases are observed whenever a major crystal plane is rotated through the beam. Figure 3 is a polar coordinate plot showing the {110} planes, the intersection of which locates the [111] axis with respect to the center of rotation, which is aligned with the beam axis.

The center of the circle in figure 3 represents the axis of rotation and and the radius corresponds to the tilt angle $\theta$. Azimuthal angles corresponding to the various planar dips in figure 2 are marked off on the circumference and connected by straight lines representing that plane in the stenogram. (Straight lines are appropriate in this case since the small conical section involved in these diagrams renders the spherical angle essentially flat.)

In the particular case shown in figure 3, coordinates of the [111] axis are $\phi$ = 270 deg, $\theta$ = 0.9 deg. At these settings the beam is aligned with the [111] axis to about 0.05 deg. However, in order to tilt the sample through the [111] axis at various values of $\phi$, the front face is adjusted *in situ* to bring the [111] axis into coincidence with the center of rotation. The long dashed lines in figure 3 represent the adjusted positions of the {110} planes, showing that the adjusted [111] axis is at the center of rotation and thus is aligned with the ion beam at $\theta$ = 0 deg for any value of $\phi$.

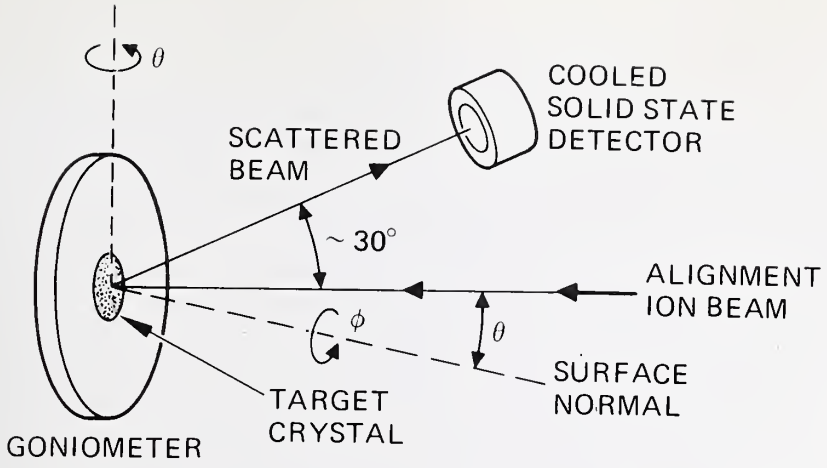


Figure 1. Schematic of target geometry used for alignment of the target crystal.

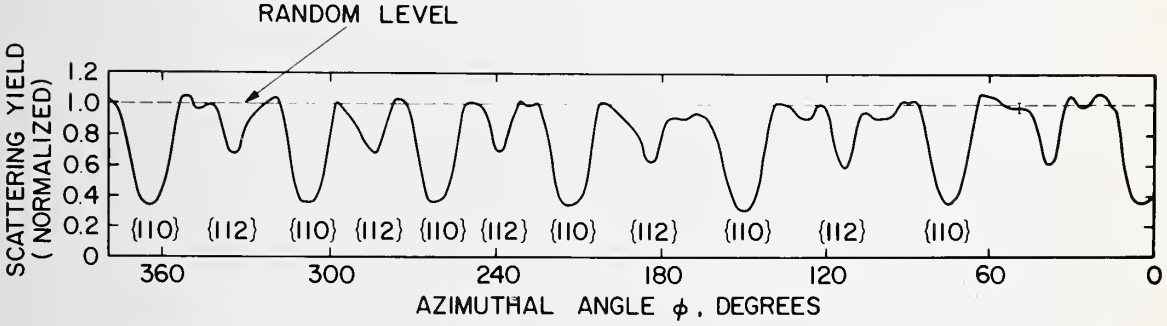


Figure 2. Scattering yield as a function of $\phi$ at constant $\theta$ = 3.5 deg for 140-keV protons incident on the (111) face of silicon. (See fig. 1 for $\phi$ and $\theta$.)

This technique assures alignment of the silicon crystal with the incident implantation ion beam to within less than 0.1 deg. The same ion beam system is used to deliver the proton beam for alignment, an alpha beam for alignment verification, and the implantation ion beam, simply by changing the species in the ion source.

The ion beam is collimated to 0.1 deg by two 5-mm diameter apertures spaced 3 m apart. The ion beam is generally focused to a 3-mm diameter spot at the target, which is located 3.5 m from the mass separator. The physical separation between beam spots differing by 1 amu is 20 mm at mass 30 and 5 mm at mass 120 when the beam collimators are removed. This indicates, for example, that with the apertures in place a $^{11}B$ beam would be free of $^{10}B$; but a $^{122}Te$ beam would be contaminated by $^{123}Te$. A contamination-free (i.e., hydrocarbons) target environment is provided by ion pumps located in both the collimator drift tube and the target chamber and by a combination of an oil-free mechanical pump and cryogenic

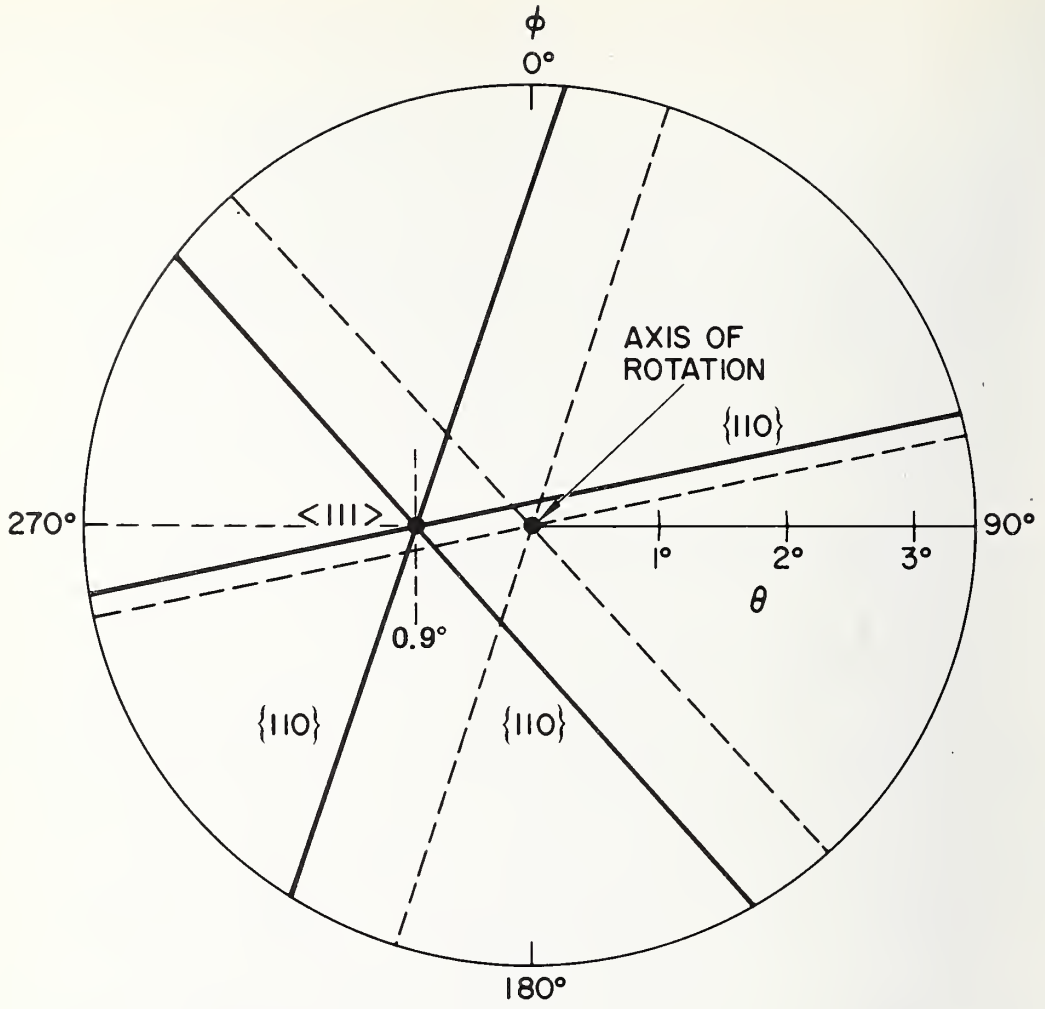


Figure 3. Polar coordinate plot of the data in figure 2 showing the {110} planes (solid lines). The intersection of the planes determines the coordinates of the [111] direction ($\phi$ = 270 deg, $\theta$ = 0.9 deg, in this case). The long dotted lines represent adjusted positions of the {110} planes showing that the [111] axis coincides with the axis of rotation after adjustment of the goniometer face.

sorption roughing, and by a cryowall at the entrance to the target chamber. The pressure in the goniometer target chamber is typically $10^{-7}$ torr.

The target goniometer is shown in figure 4. The orientation of the silicon crystal is adjusted by a stepping motor driven system controlled from outside the vacuum system. Three independent angular variations are possible. A tilt angle $\theta$ about a vertical axis through the target face is introduced through the large horizontal gear which can be seen in the photograph. Rotation in azimuth about a horizontal axis is introduced through the vertical disk to which the crystal is attached. The disk is adjusted *in situ* by means of the three peripheral screws to permit the

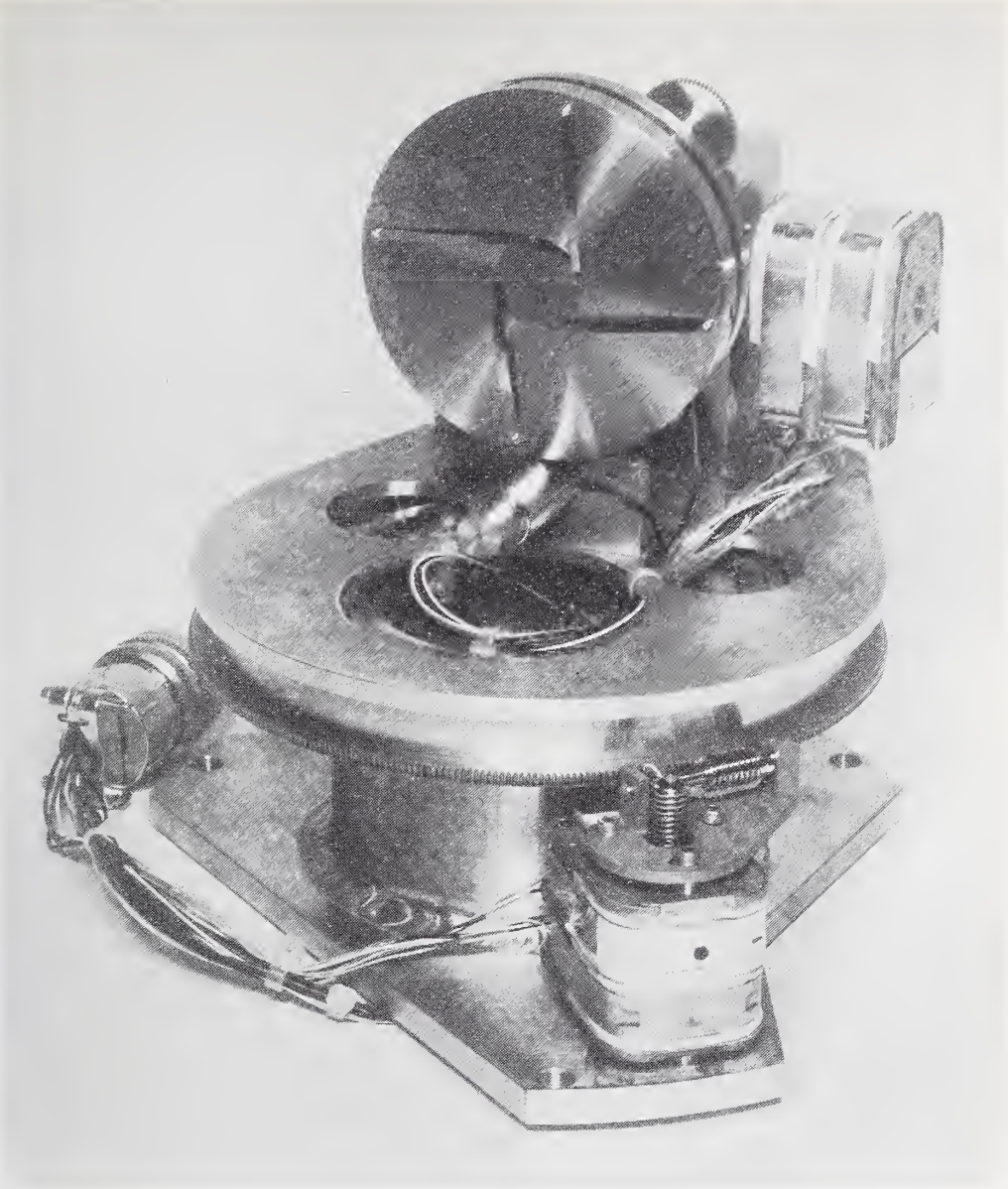

Figure 4. Target goniometer for alignment and angular control.

introduction of the third independent angular displacement. Counters, driven by slave motors, display the angular position of the stepping motor drives to within 0.02 deg. Stepping rates of up to a maximum of 80 per second are controllable by the operator in eight speed ranges and two directions. At the maximum stepping rate an entire rotation can be traversed in about 4.5 min. The speed is controlled electrically by means of an oscillator which drives a flip-flop, which in turn drives a pulsing circuit. The angle between the incoming ions and the desired silicon crystal direction is thus controlled to <0.1 deg and the sample-tilt angle can be varied and controlled to about 0.02 deg. The angular

control accuracy for implanted depth distributions obtained for samples aligned by this technique is therefore <0.1 deg.

For the larger angles, the silicon samples were simply tilted to the desirable angle by rotating the target mount in a routine implantation system with the silicon sample oriented so that the tilt occurs in the direction toward the random equivalent (e.g., 7-deg tilt about the vertical axis, with a (110) plane rotated 18 deg from the vertical for a (111) wafer.)

In the case of the technique used for the larger angle, the accuracy of alignment depends on several factors in combination. The silicon samples are cut and polished to be within about 0.5 to 1 deg of the designated crystal face. The target holder can be positioned to within about 0.5 deg of the desired angle between 0 and 7 deg. Ion beam scanning produces an angular deviation over a standard test sample area (6 mm square around the center) of 0.2 deg. Thus, the first of these is the greatest and the combination of all errors should cause a deviation between the direction of the incident ions and the desired crystal direction of ∿1 deg, absolute.

### 2.3 Characterization of Depth Distribution Variation with Alignment Angle

It was necessary to devise a method to characterize the change in depth distribution of carrier concentration with alignment angle as the profiles were varied from maximum (optimal) channeling conditions to minimum channeling conditions. The technique selected was to measure the differential integrals of the areas between the various depth distributions as illustrated in figures 5 and 6. Figure 5 represents the determination of the extent of channeling and dechanneling for the case of an implant with angular alignment which yields intermediate amounts of channeling. The optimally channeled profile can only be determined empirically; however, the minimum channeling distribution can be estimated by using the Gaussian approximation to the LSS random distribution [8]. Thus, the magnitude of the channeling tail is the fraction of the implanted dose that penetrates beyond the Gaussian approximation to the LSS random distribution (i.e., the area integral ①); while the extent of dechanneling is the fraction of the implanted dose that is lost from the optimally channeled distribution (i.e., the area integral ②). The choice of the Gaussian approximation to represent the random distribution neglects the contribution of higher order moments in the solution of the LSS range equations. These higher order moments are responsible for the skewed nature of implants in amorphous silicon or in high dose (amorphizing) implants into initially crystalline silicon. Although neglect of these higher order moments can lead to variations of 10 to 15 percent between the Gaussian approximation and actual random impurity distributions in noncrystalline silicon for which the possibility of ion channeling is eliminated, only small skewness is observed in this study for these low fluence implants into crystalline silicon. The uncertainty due to the neglect of higher order moments is small compared with the great variations encountered in random yield as the substrate is rotated away from

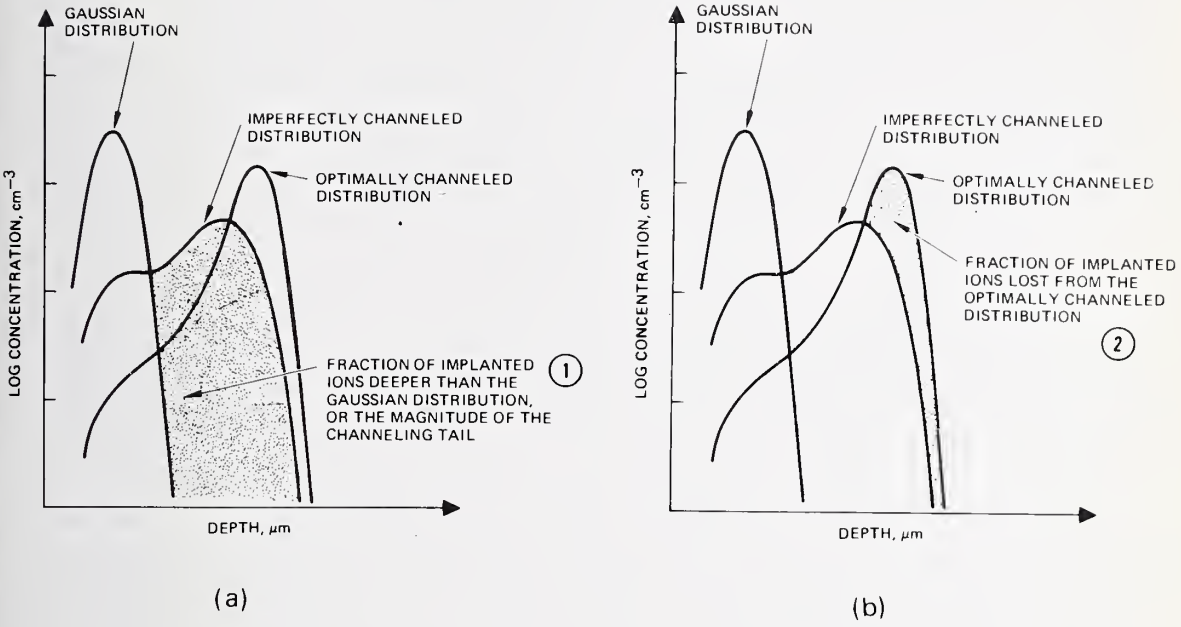


Figure 5. Example of the determination of the area integrals chosen for data reduction for the case of an imperfectly channeled distribution. (a) The area integral used to estimate channeling is the fraction of the total number of implanted ions that penetrate beyond the Gaussian approximation to the random distribution. (b) The area integral used to estimate dechanneling is the fraction of the total number of implanted ions that no longer fall within the optimally channeled distribution.

low index crystallographic orientations toward the beam direction. The number of ions lost from the optimally channeled distribution is developed by the area integral ②. The use of the term "optimally channeled" is justified because the accuracy of angular control in this work is 0.05 deg and the depth distributions are shown in this work not to change until the alignment angle exceeds about 0.3 to 0.5 deg from axial alignment. This angle of 0.3 to 0.5 deg is defined as $\psi_o$, the critical dechanneling angle (see fig. 6). A representative plot of the fractions ① and ② as a function of alignment angle is shown in figure 6 for 300-keV boron in (110) silicon. Curve ① which plots the relative magni-

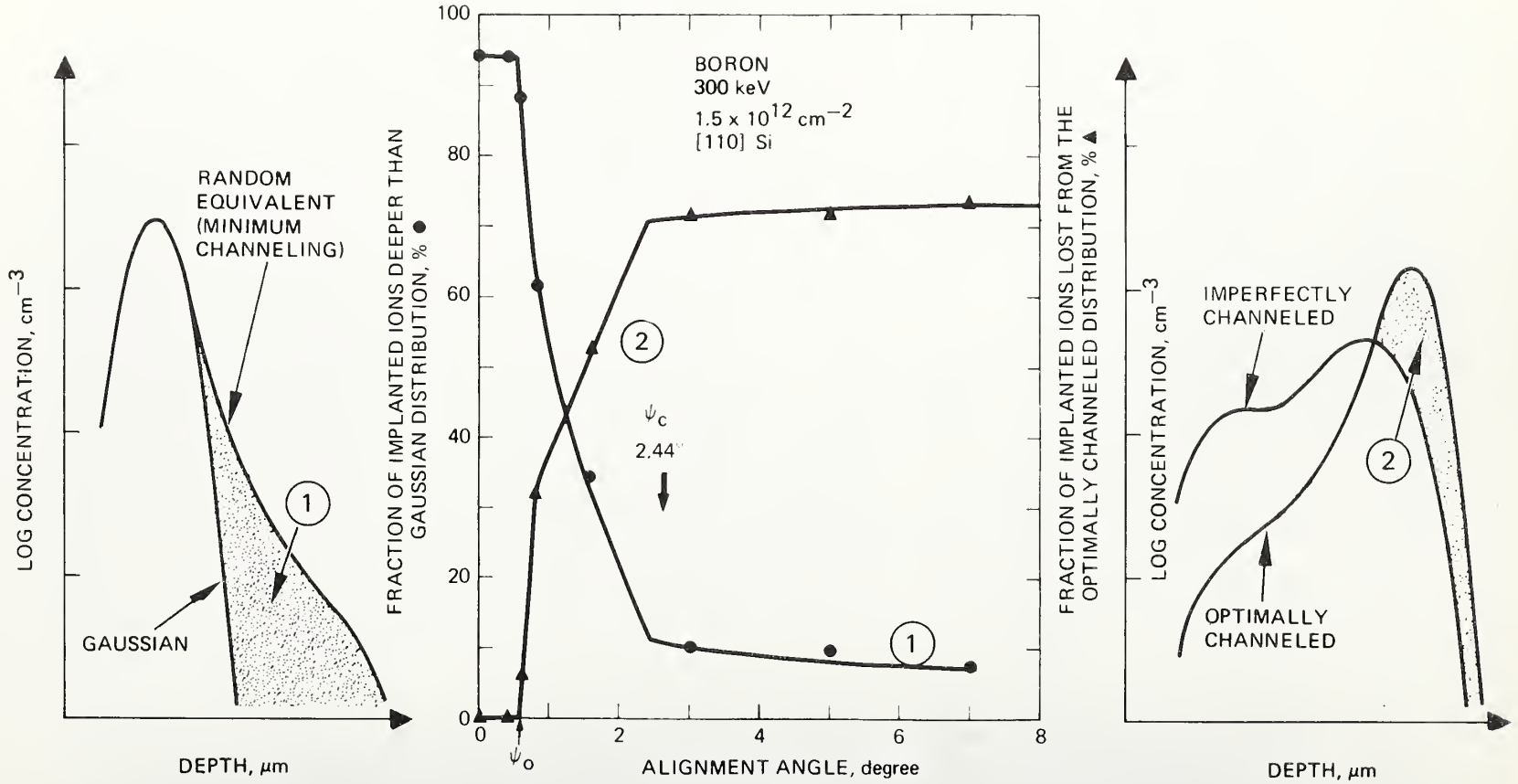


Figure 6. Explanation of regions of implanted depth distributions.

tude of area ① shows that a maximum number of ions is channeled as long as the alignment angle is less than $\psi_o$. As the alignment angle is increased beyond $\psi_o$, more and more ions are dechanneled, thereby building up the random distribution and reducing the number of ions in the channeled distribution. At sufficiently large angles, all of the ions are scattered, mostly into a random distribution, although a small number may be deflected to follow channeled paths. Curve ②, which plots the relative magnitude of the area ②, shows that no ions are lost from the optimally channeled distribution in the region from perfect alignment ($\psi = 0$) to the critical dechanneling angle $\psi_o$. Then, as the alignment angle is increased, ions are lost into the lattice by nuclear scattering. Finally, the only ions that penetrate beyond the random distribution are those that are deflected into channels.

## 3. EXPERIMENTAL RESULTS

The data obtained in this study are summarized in table 1 for the ion-energy orientation combinations examined. Examples of the depth distribution of electrical activity versus alignment angle (the angle between the ion beam and the nearest low index silicon crystallographic direction) for alignment angles from 0 to 7 deg are shown in figures 7 through 15, for nine of the ion-energy-orientation combinations listed in table 1. From these profiles several trends in the data become obvious. Channeled implantations lead to increased penetration depths, with the peak of the perfectly channeled distribution occurring at depths that vary from 1.5 times deeper than the random peak (for 300-keV boron into (111) silicon) to as much as 30 times deeper than the random peak (for 75-keV arsenic into (110) silicon). Along with the variation in penetration depths from channeled to random implants, there is also a significant change in the shape of the resulting ion distributions as the angle of incidence for the beam is altered. Finally, the depth of the near-surface peak in electrical activity changes as the angle of incidence is varied. As is discussed in 4.4.3, the near-surface peak is not due solely to ions that follow a random trajectory, and thus does not always occur at the depth predicted by range theory for amorphous targets.

The data provided by these experiments for all the combinations of table 1 were analyzed as described in 2.3. and the results plotted versus the angle of incidence. (The critical angle, as calculated in Appendix A, is also indicated.) Representative results are shown in figures 16 through 23. In the curves shown in figures 18 through 22, the solid data points represent accurate alignment and were obtained using Rutherford backscattering; the open data points for the less sensitive larger angles were obtained by tilting the target holder. Data given in [5] for 450-keV phosphorus were also analyzed and plotted in a similar manner; the results are shown in Appendix B. When the data are plotted in this manner, several additional trends become apparent. The angle at which the random yield increases to a value halfway between the value for 0-deg incidence and the saturation random yield is referred to as $\psi_{1/2}$. This angle is seen to vary from approximately 0.8 $\psi_c$ to $\psi_c$. In addition, the random fraction is seen to saturate when the alignment angle is between 1.6 $\psi_c$

Table 1. Implantation Angular Control Data

| $\psi_c$ deg | Energy keV | Ion | Silicon Orientation | Random Fraction at 7 deg % | $\psi_o$[a] deg | Fraction Not in Distribution at 1 deg Off Axis % | Same at 2 deg Off Axis % |
|---|---|---|---|---|---|---|---|
| 1.97 | 300 | B | 100 | 97.3 | 0.3 | 40 | 54 |
| 2.16 | 300 | B | 111[b] | 93.9 | 0.4 | 39 | 56 |
| 2.33 | 450 | P | 100[b] | 93.0 | ~ 0.2 | 60 | 67 |
| 2.44 | 300 | B | 110[b] | 92.4 | 0.6 | 38 | 62 |
| 2.57 | 450 | P | 111[b] | 95.0 | ~ 0.2 | 48 | 67 |
| 2.94 | 450 | P | 110[b] | > 90 | ~ 0.2 | 58 | 72 |
| 2.95 | 300 | As | 100 | 86.9 | ~ 0.2 | 12 | 25 |
| 3.12 | 75 | B | 100 | 87.8 | 0.45 | 38 | 59 |
| 3.29 | 300 | As | 111 | 87.4 | 0.35 | 12 | 23 |
| 3.40 | 300 | In | 111 | - | - | 14 | 29 |
| 3.45 | 75 | B | 111 | 86.7 | 0.7 | 16 | 34 |
| 3.84 | 300 | As | 110 | 84.1 | 0.6 | 11 | 31 |
| 3.92 | 150 | In | 111 | 63.0 | - | - | 37 |
| 3.98 | 75 | B | 110 | 89.7 | 0.4 | 19 | 36 |
| 3.98 | 300 | In | 110 | 75.0 | 0.3 | 16 | 37 |
| 4.00 | 150 | Al | 110 | 92.7 | 0.35 | 22 | 45 |
| 4.41 | 75 | As | 111 | 46.5 | ~ 0.6 | 7 | 18 |
| 4.61 | 150 | In | 110 | - | ~ 0.4 | 6 | 21 |
| 4.79 | 20 | B | 111 | 73.0 | - | 5 | 8 |
| 5.19 | 75 | As | 110 | 61.6 | ~ 0.3 | 8 | 21 |
| 5.22 | 40 | In | 111 | 57.0 | - | ~ 12 | ~ 22 |
| 5.32 | 75 | In | 110 | 56.5 | - | 15 | 28 |
| 5.61 | 20 | B | 110 | 71.4 | - | 12 | 15 |
| 5.87 | 20 | As | 111 | 24.0 | - | 3 | 5 |
| 6.10 | 40 | In | 110 | 31.3 | - | 11 | 17 |
| 6.86 | 20 | As | 110 | 23.9 | - | 4 | 7 |

[a] $\psi_o$ is defined here as the angle at which deviation from the optimally channeled distribution begins, and is called the critical dechanneling angle.

[b] From Reddi and Sansbury [5].

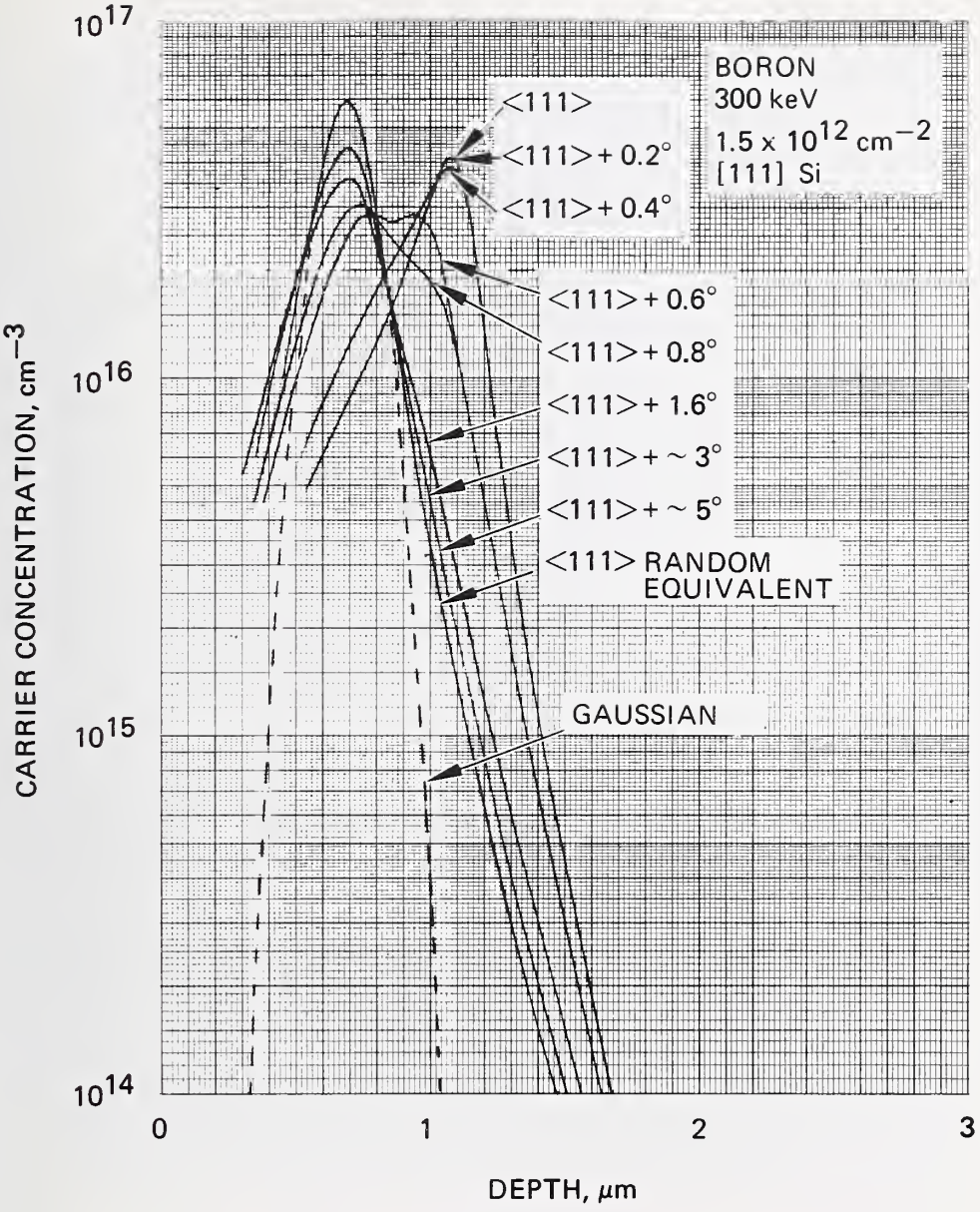


Figure 7. Depth distributions of carrier concentration as a function of alignment angle for 300-keV boron in (111) silicon.

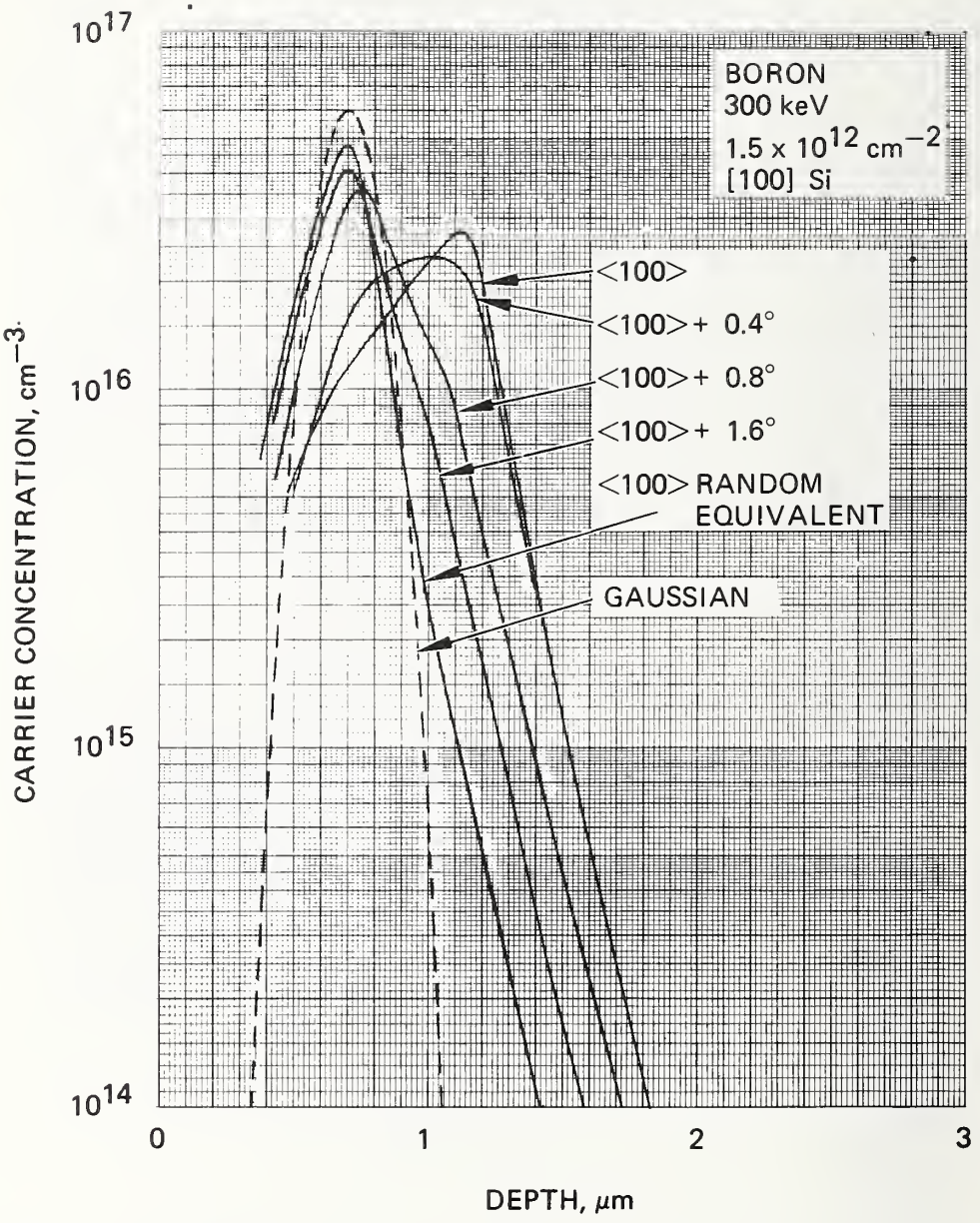


Figure 8. Depth distributions of carrier concentration as a function of alignment angle for 300-keV boron in (100) silicon.

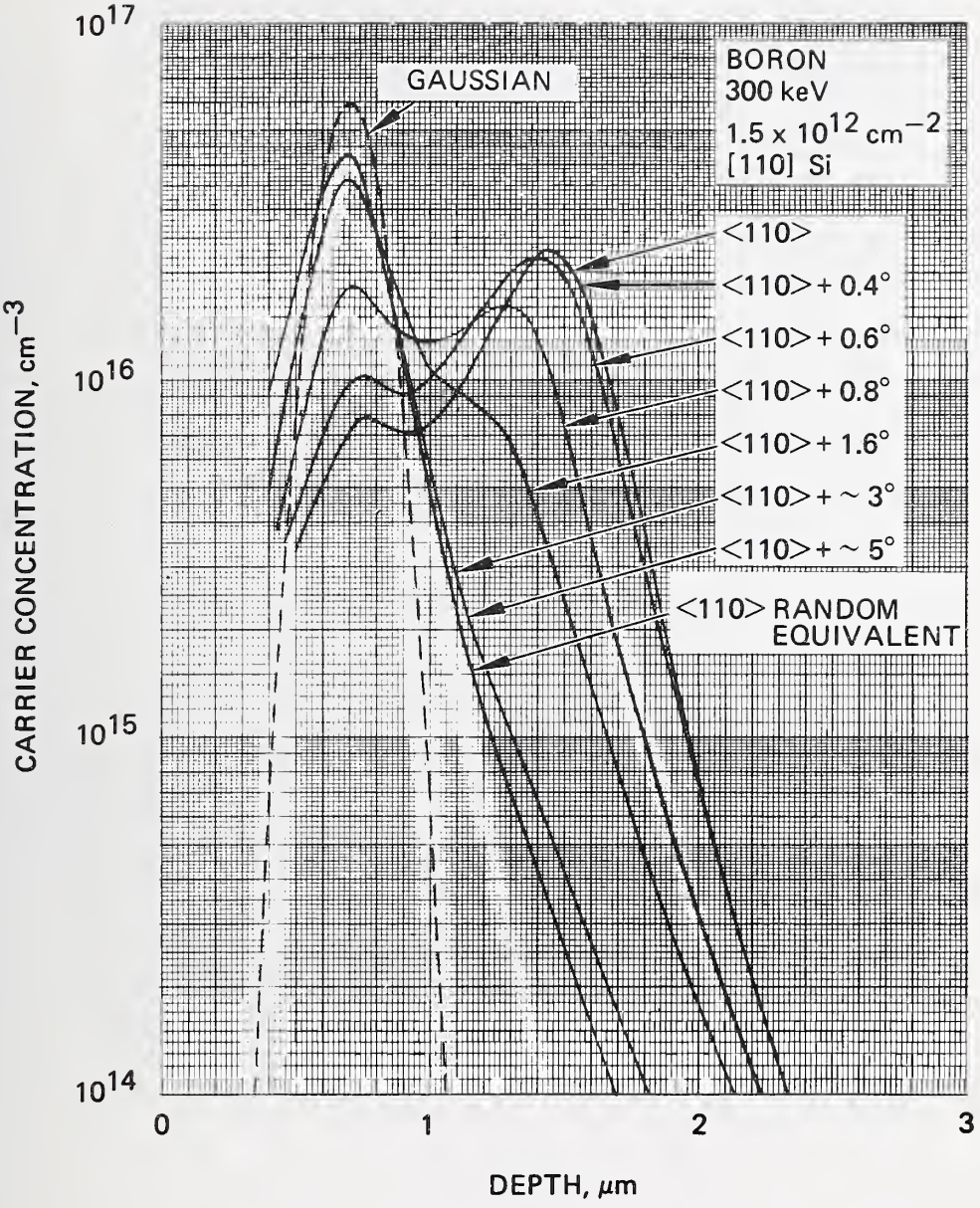


Figure 9. Depth distributions of carrier concentration as a function of alignment angle for 300-keV boron in (110) silicon.

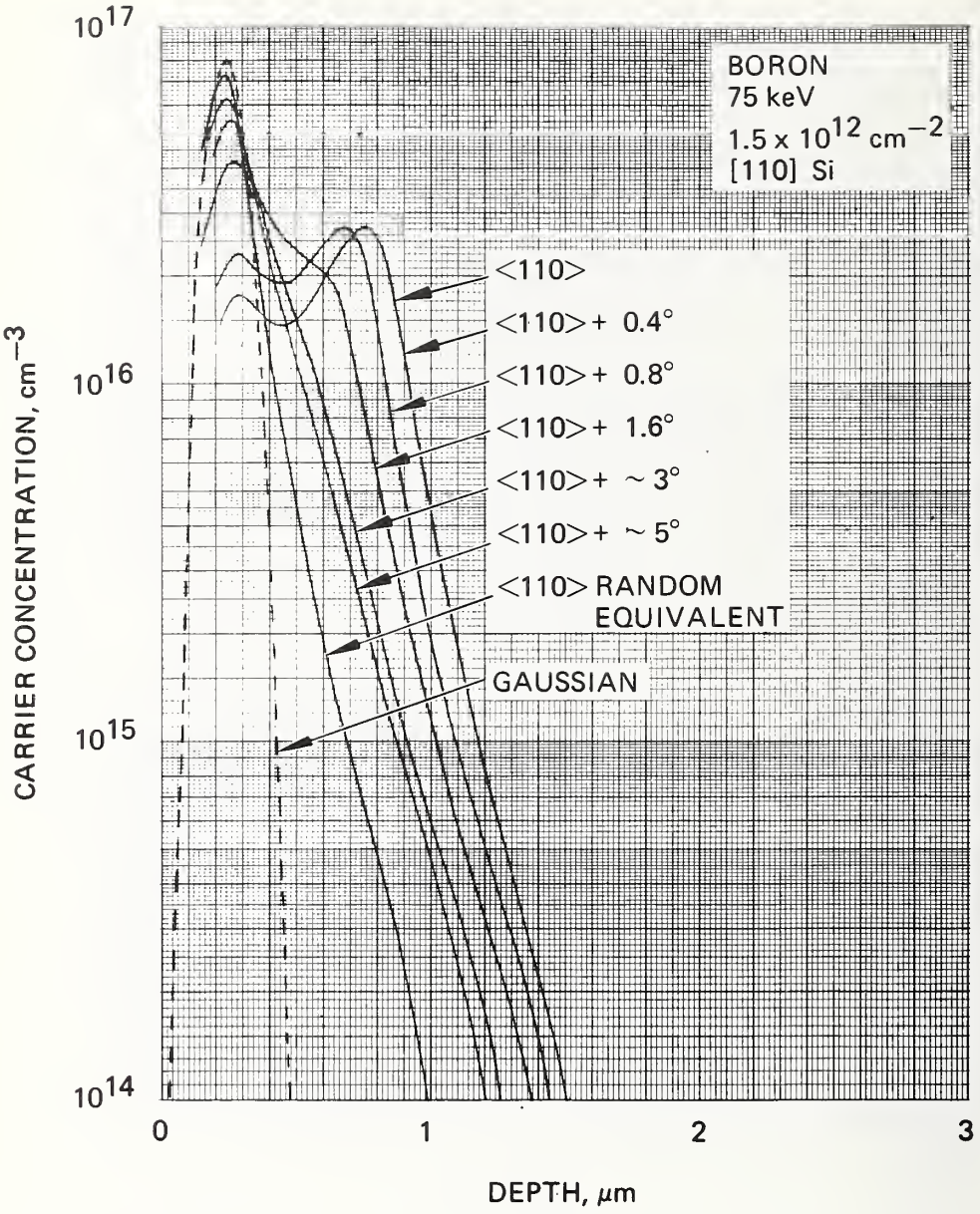


Figure 10. Depth distributions of carrier concentration as a function of alignment angle for 75-keV boron in (111) silicon.

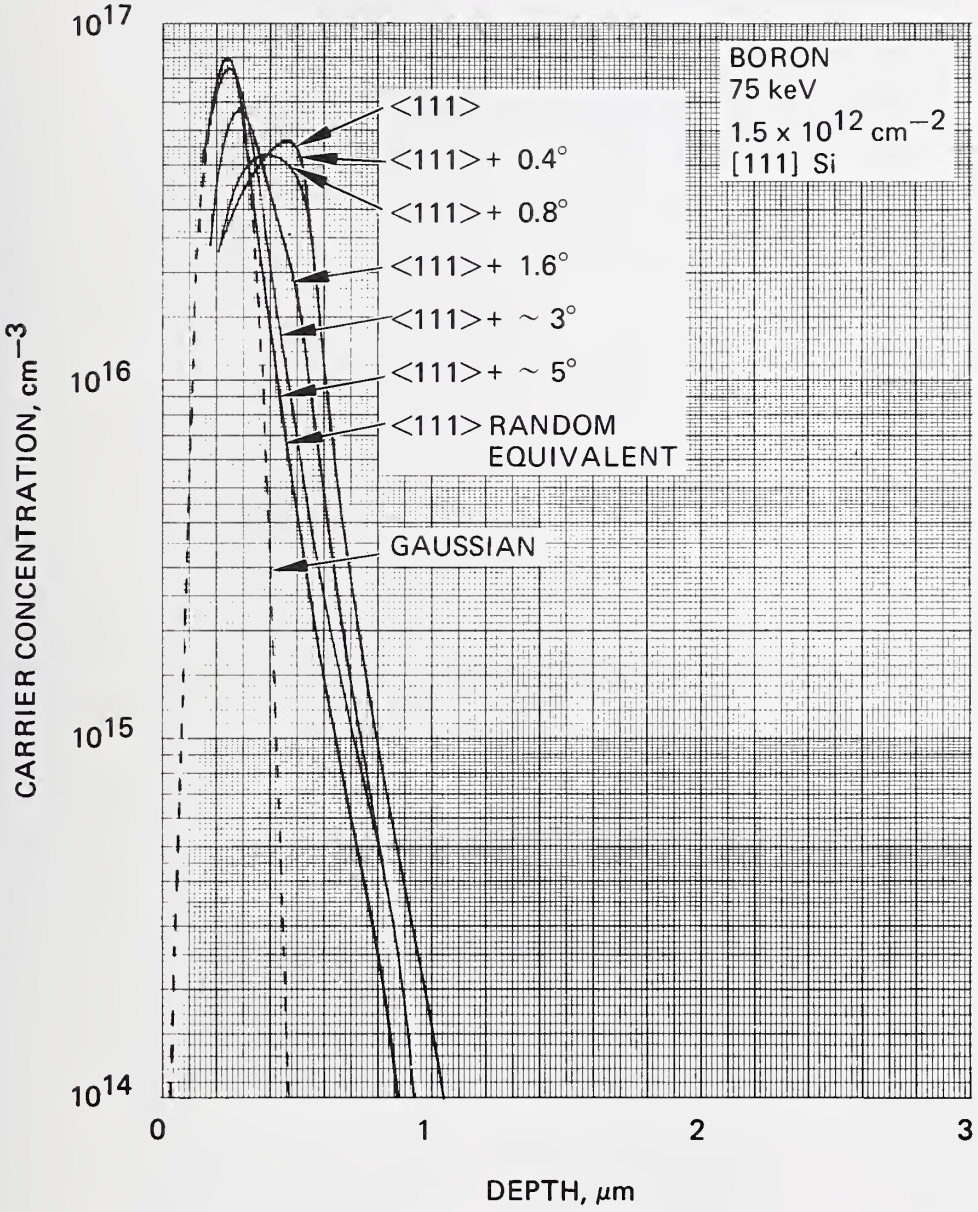


Figure 11. Depth distributions of carrier concentration as a function of alignment angle for 75-keV boron in (110) silicon.

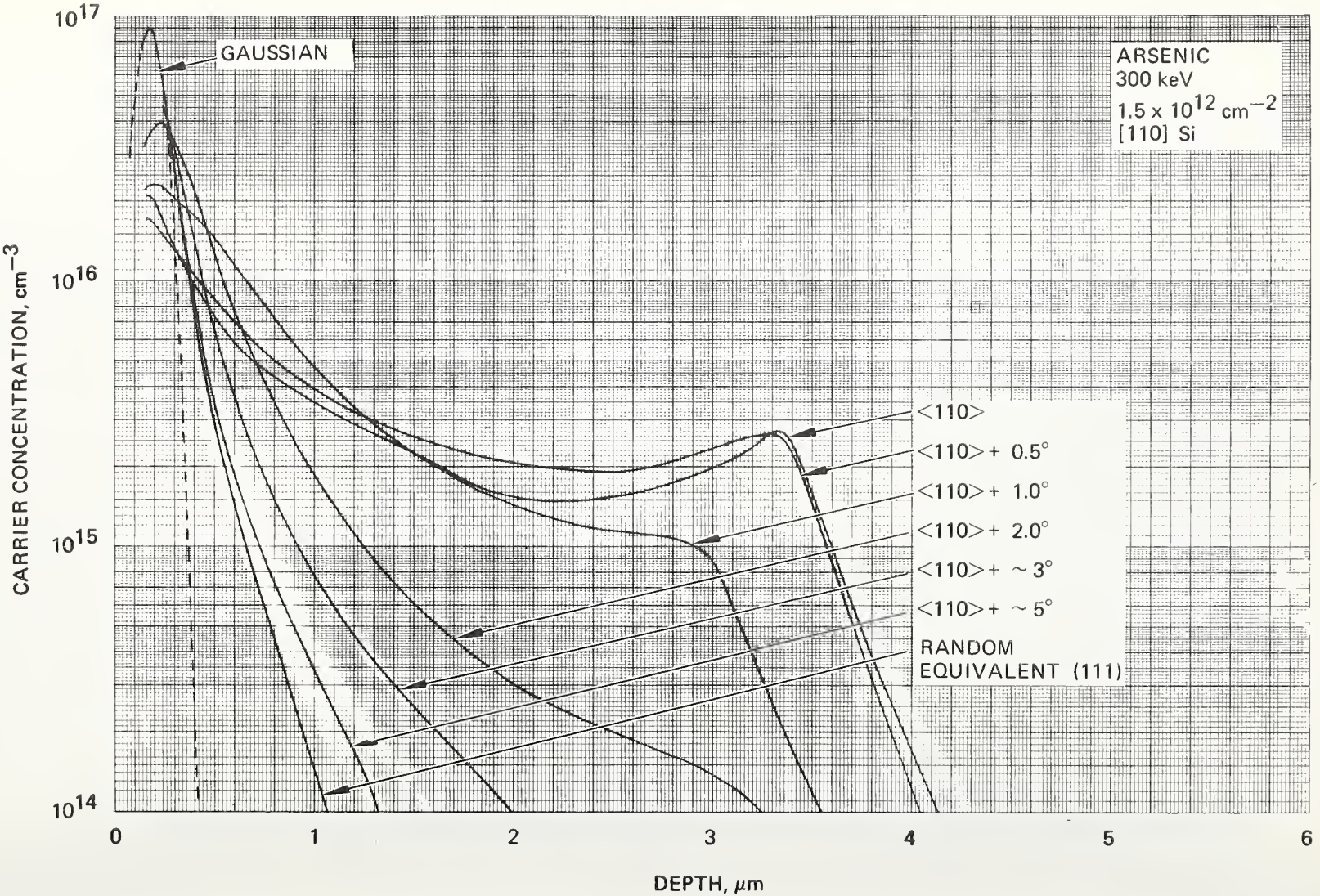


Figure 12. Depth distributions of carrier concentration as a function of alignment angle for 300-keV arsenic in (110) silicon.

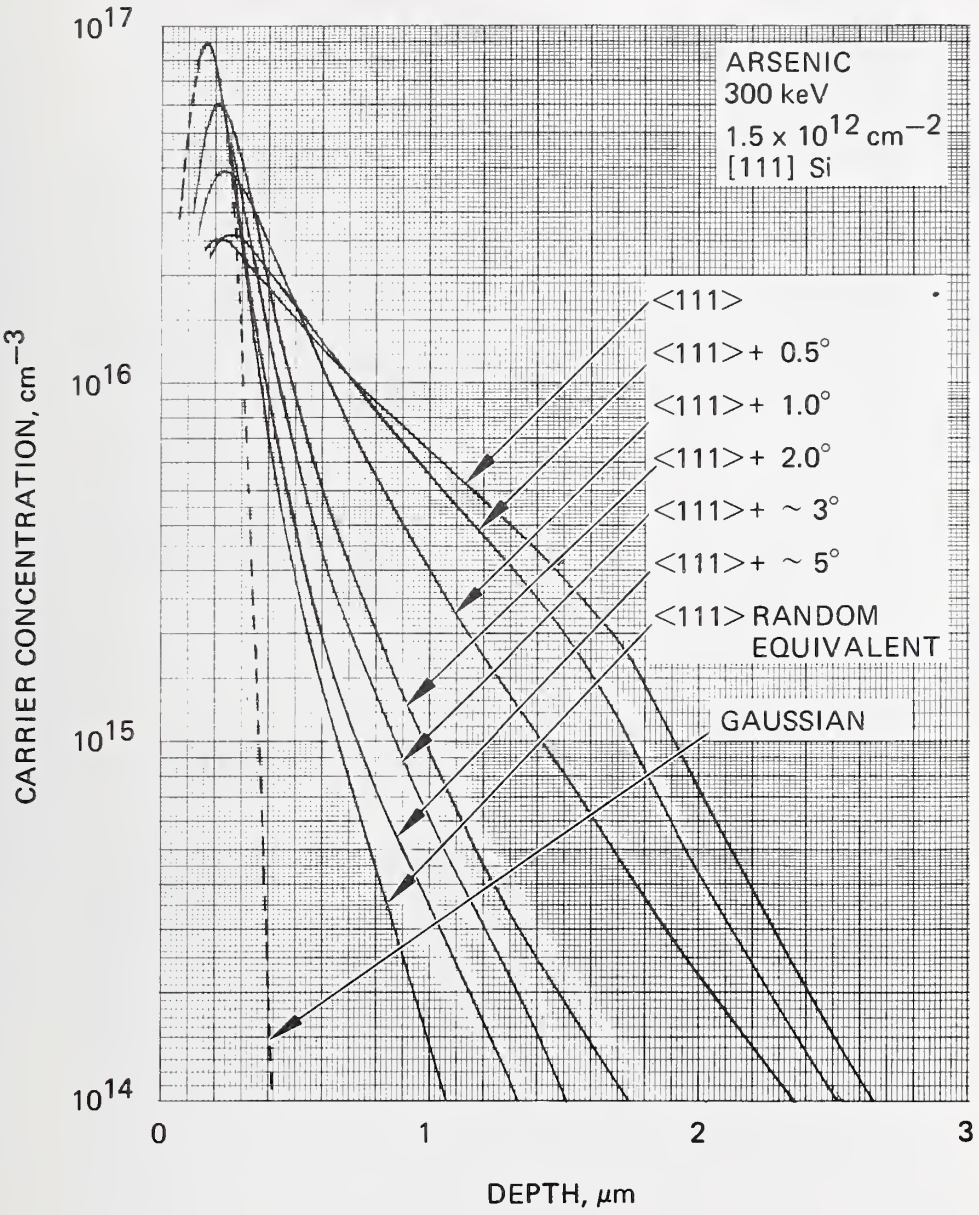


Figure 13. Depth distributions of carrier concentration as a function of alignment angle for 300-keV arsenic in (111) silicon.

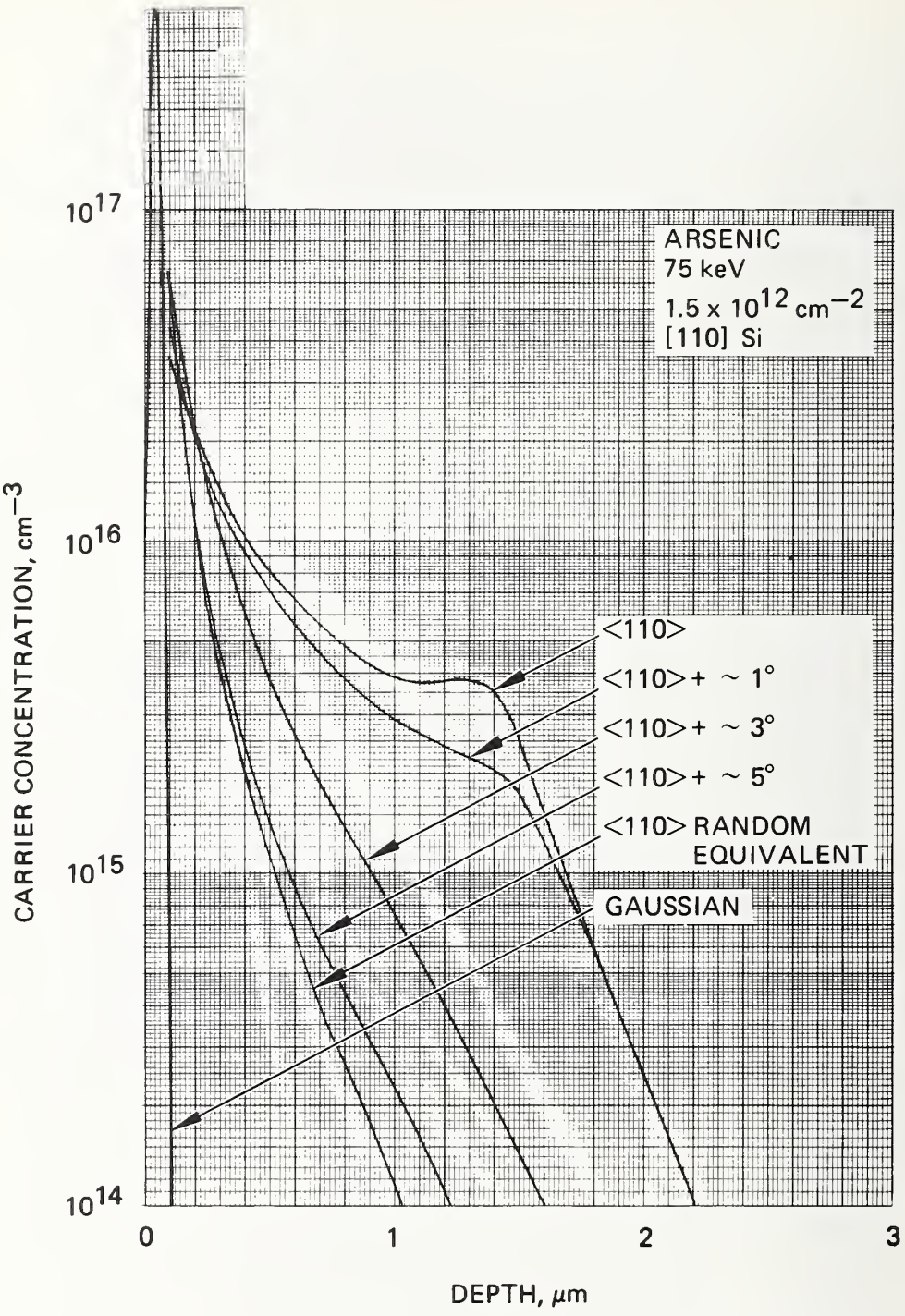


Figure 14. Depth distributions of carrier concentration as a function of alignment angle for 75-keV arsenic in (110) silicon.

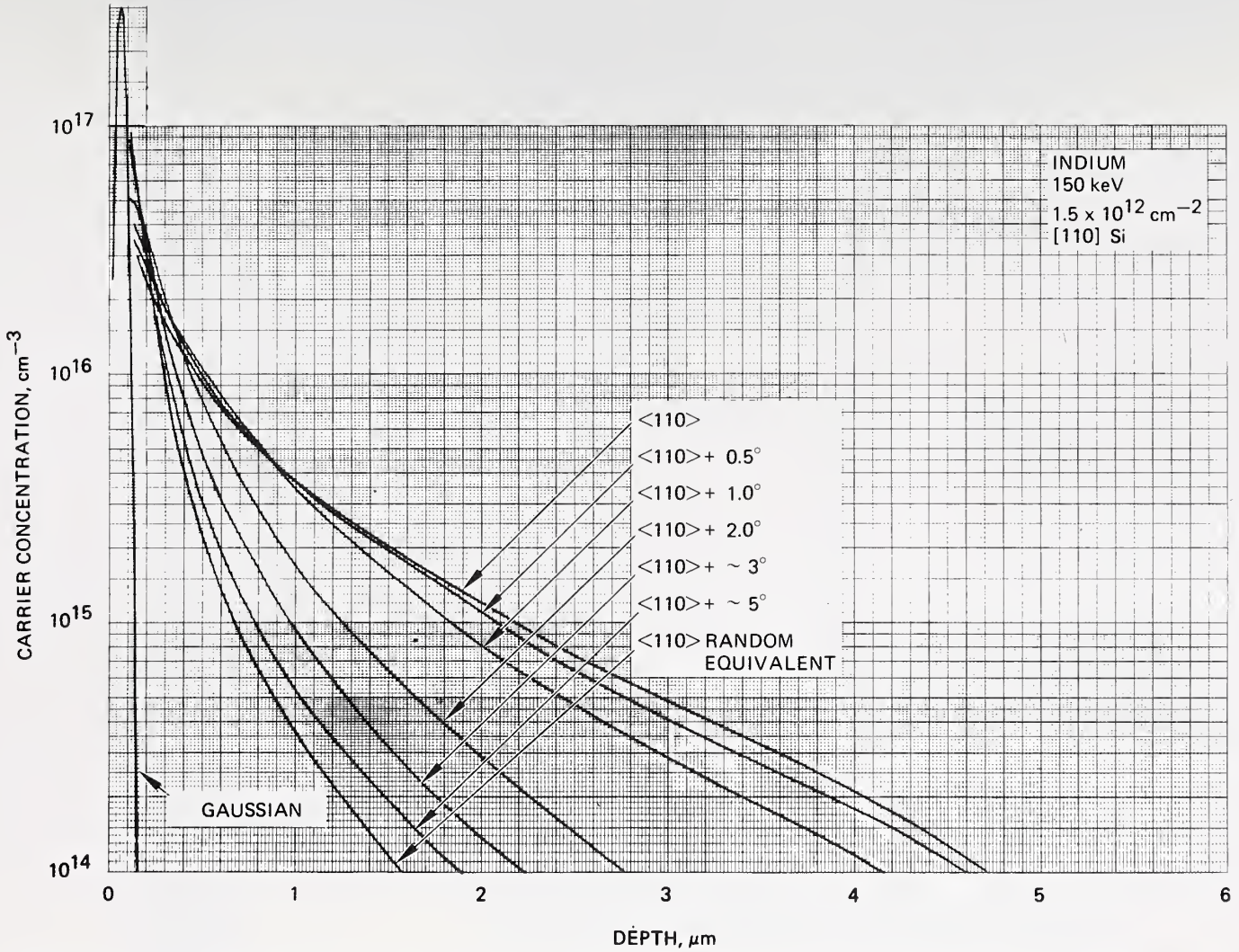


Figure 15. Depth distributions of carrier concentration as a function of alignment angle for 150-keV indium in (110) silicon.

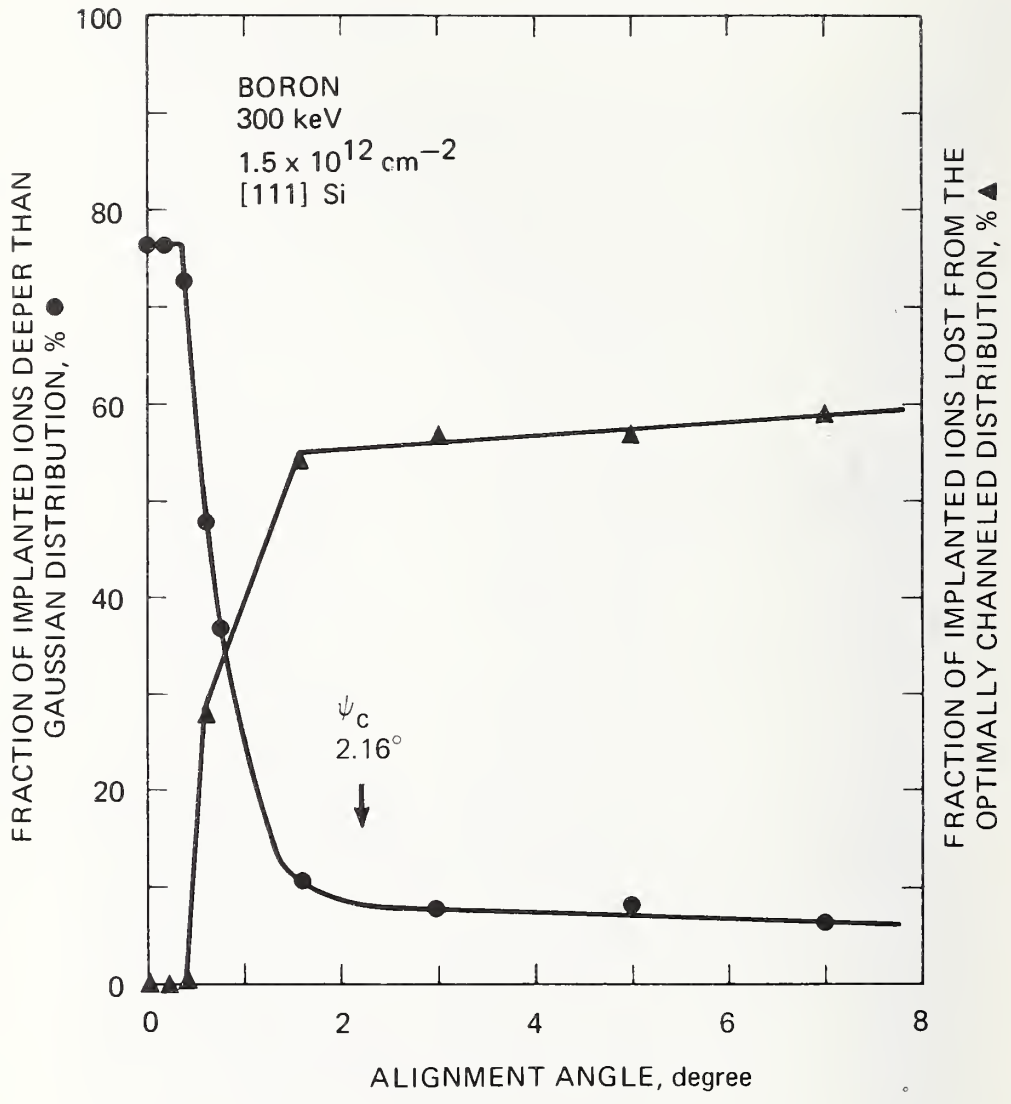


Figure 16. Magnitudes of channeling and dechanneling versus alignment angle for 300-keV boron in (111) silicon. (Error bars are not indicated on the figure; experimental uncertainties are described in the text.)

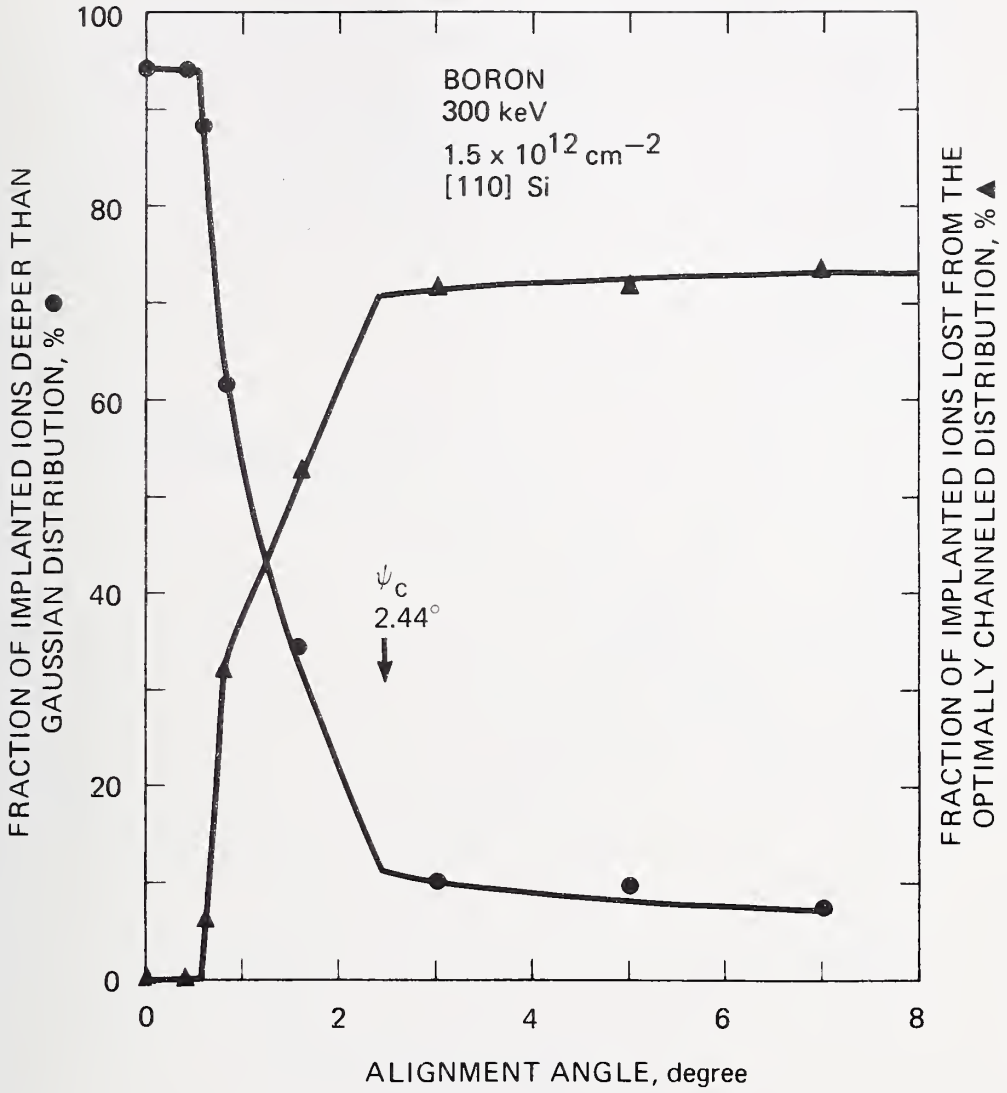


Figure 17. Magnitudes of channeling and dechanneling versus alignment angle for 300-keV boron in (110) silicon. (Error bars are not indicated on the figure; experimental uncertainties are described in the text.)

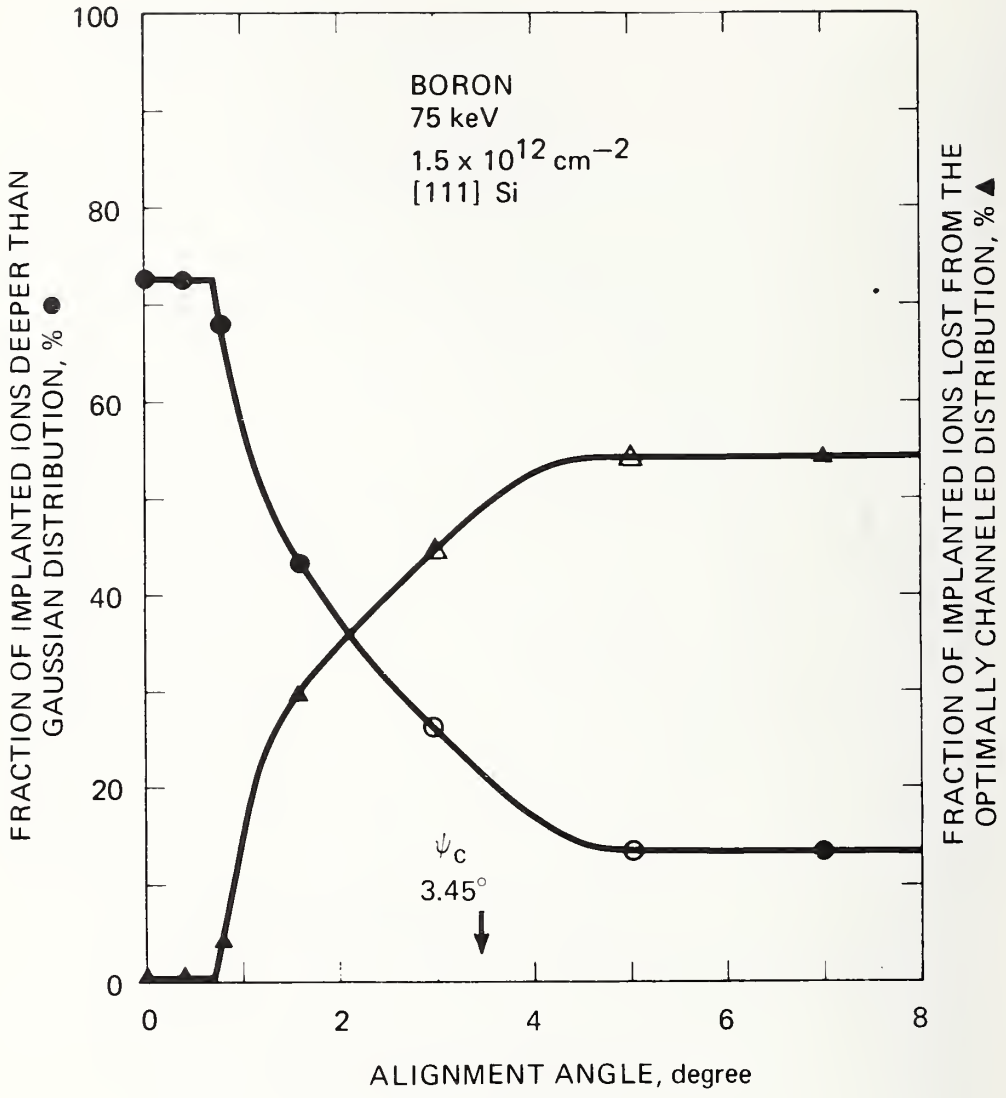


Figure 18. Magnitudes of channeling and dechanneling versus alignment angle for 75-keV boron in (111) silicon. (Error bars are not indicated on the figure; experimental uncertainties are described in the text.)

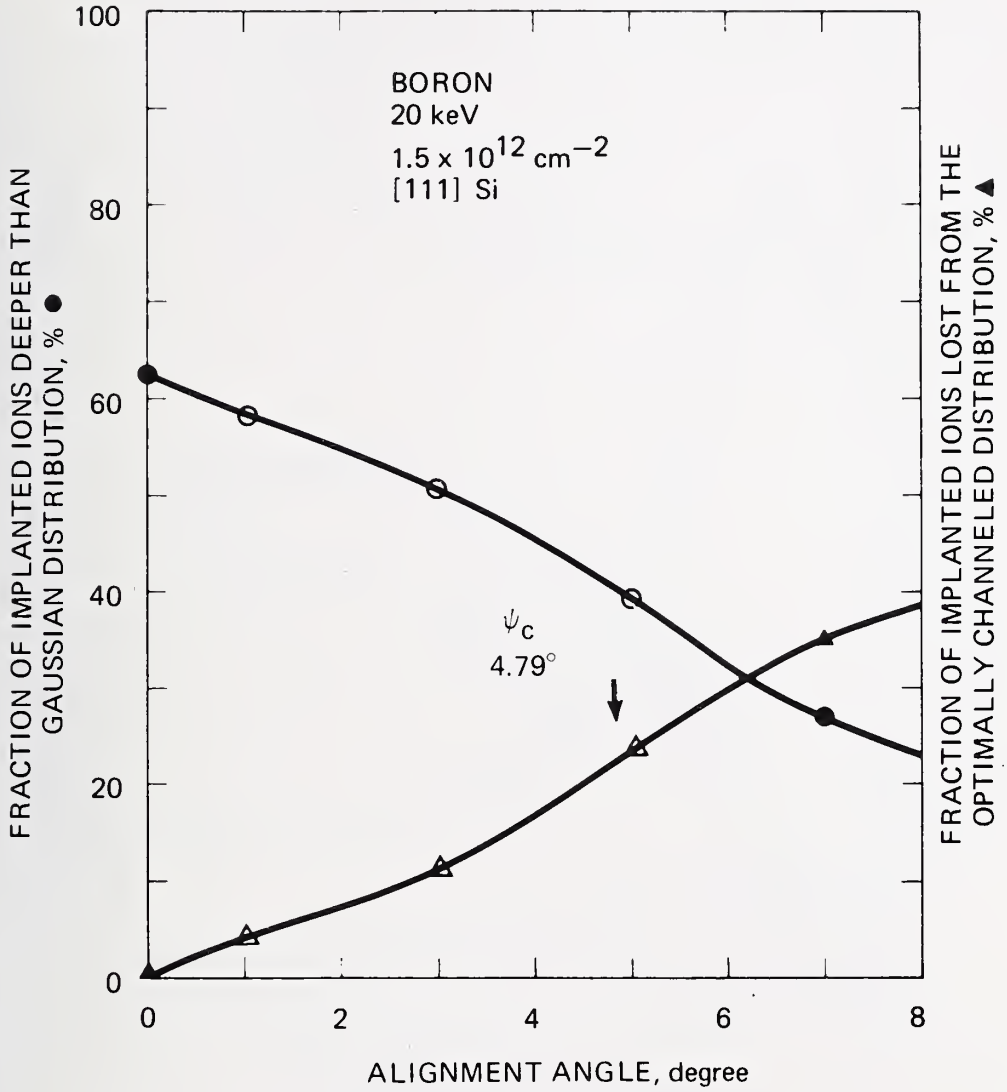


Figure 19. Magnitudes of channeling and dechanneling versus alignment angle for 20-keV boron in (111) silicon. (Error bars are not indicated on the figure; experimental uncertainties are described in the text.)

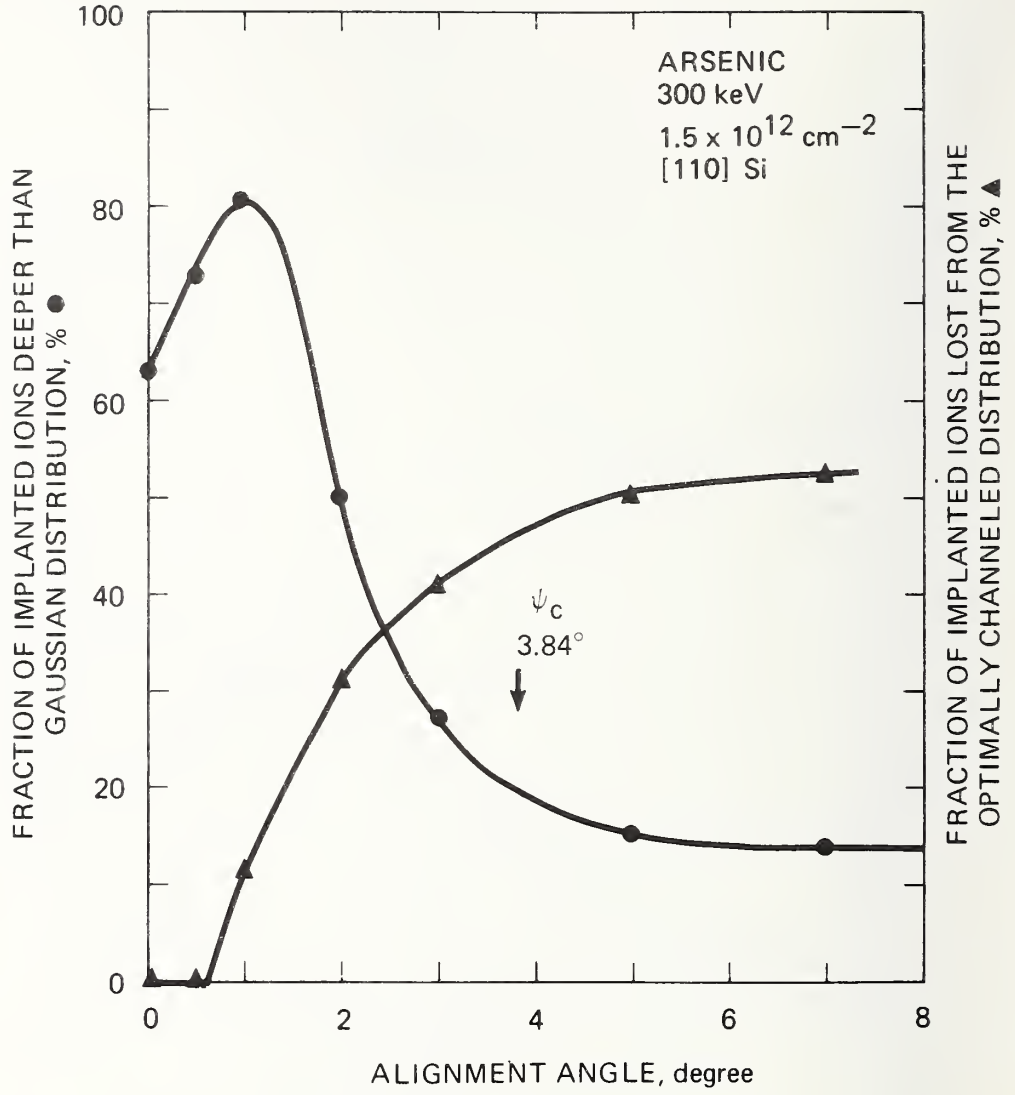


Figure 20. Magnitudes of channeling and dechanneling versus alignment angle for 300-keV arsenic in (110) silicon. (Error bars are not indicated on the figure; experimental uncertainties are described in the text.)

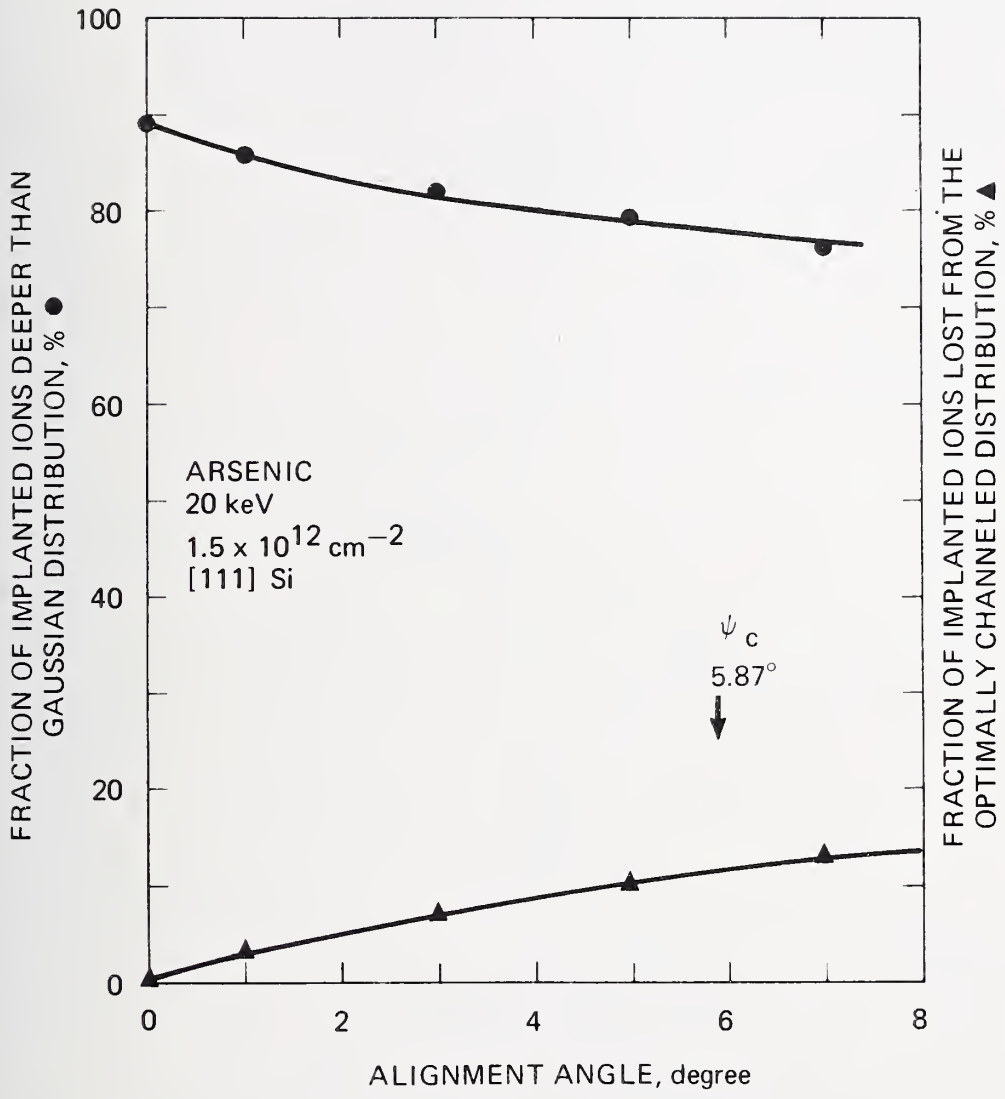


Figure 21. Magnitudes of channeling and dechanneling versus alignment angle for 20-keV arsenic in (111) silicon. (Error bars are not indicated on the figure; experimental uncertainties are described in the text.)

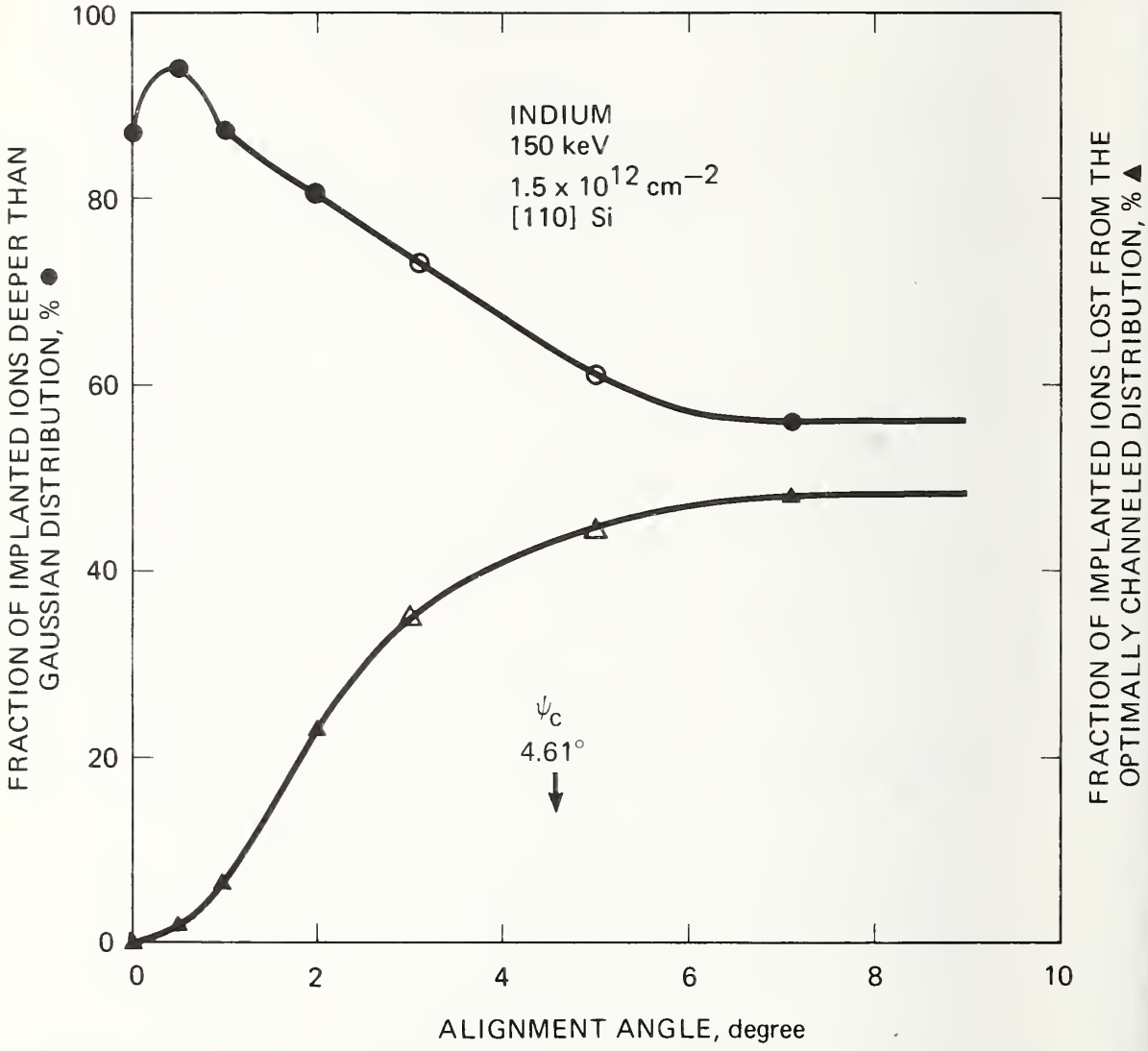


Figure 22. Magnitudes of channeling and dechanneling versus alignment angle for 150-keV indium in (110) silicon. (Error bars are not indicated on the figure; experimental uncertainties are described in the text.)

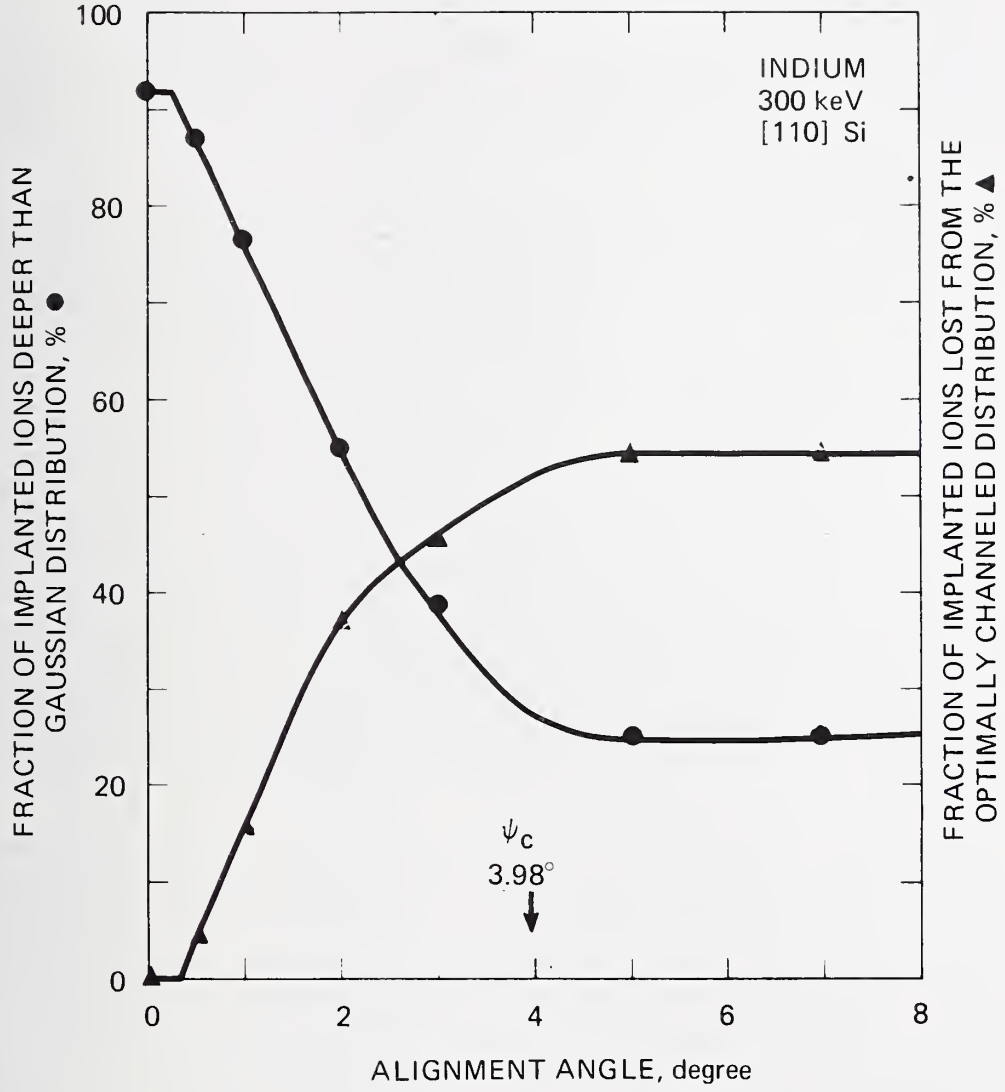


Figure 23. Magnitudes of channeling and dechanneling versus alignment angle for 300-keV indium in (110) silicon. (Error bars are not indicated on the figure; experimental uncertainties are described in the text.)

to 2 $\psi_c$. (Recall that the substrate angles are uncertain by 0.7 deg for alignment angles greater than 3 deg.) The fraction of the random equivalent distribution deeper than the Gaussian approximation to the amorphous distribution is given in column 5 of table 1. (Recall that these values may be in error by a few percent in estimating the true random fraction due to the neglect of higher-order moments in the solution to the LSS equations.) These data are plotted versus the ratio of alignment angle to the critical angle in figure 24. These data also show a saturation of random yield for $\psi = 2\ \psi_c$.

The sensitivity of the channeled distributions to angular alignment is demonstrated in columns 7 and 8 of table 1. Column 7 presents the fraction of the implanted ions lost from the optimally channeled distribution for an alignment angle of 1 deg, while column 8 presents the fraction of the implanted ions lost from the optimally channeled distribution for an alignment angle of 2 deg. These data show that within the error due to neglect of higher order moments the implants characterized by a smaller critical angle are more sensitive to angular alignment, as expected. Column 6 is $\psi_o$, the approximate angle at which the channeling distribution begins to deviate from the optimally channeled distribution; and the angle is called the critical dechanneling angle. This angle is most likely the angle at which the ion trajectory begins to deflect out of a single axial channel and wanders among several axial channels (as is described in 4.1.). Moline and Reutlinger [4] have also noted that this angle is just less than 0.5 deg for the isolated case of 100- and 300-keV phosphorus. From the data presented in this table, the ion beam must be controlled to be within 0.5 ± 0.2 deg to guarantee that the optimally channeled depth distribution for implantations directly into low index crystallographic orientations is obtained.

One set of SIMS atomic profiles was measured for comparison with the C-V carrier profiles. SIMS profiling was accomplished by rastering a 5-keV 2.5- to 5-nA $O_2^+$ beam over a region of the sample surface with secondary ions accepted only over the crater center. The depth scale was determined by averaging a series of measurements of the crater depth using a surface profilometer and sampling the crater from several different directions, while the concentration scale was determined by setting the integrated secondary ion yield equal to the known ion fluence. A background subtraction was performed to eliminate the effects of residual interferences. The case selected was 150-keV boron in (110) silicon. The material, alignment technique, implantation conditions, and annealing conditions were identical except that the ion fluence for the SIMS measurement was $1 \times 10^{13}$ cm$^{-2}$, while that for the C-V measurements was $1.5 \times 10^{12}$ cm$^{-2}$. This difference in ion fluence was dictated by the relative sensitivities of the two measurement techniques and could account for some difference in shape of depth distribution because of the randomizing effects of the greater damage in the higher fluence implant for SIMS. Both fluences are low relative to the amorphization fluence and the annealing condition of 800°C for 20 min is not likely to cause significant redistribution. The data from the SIMS measurement are shown in figure 25. Data for four alignments are shown in order to give repre-

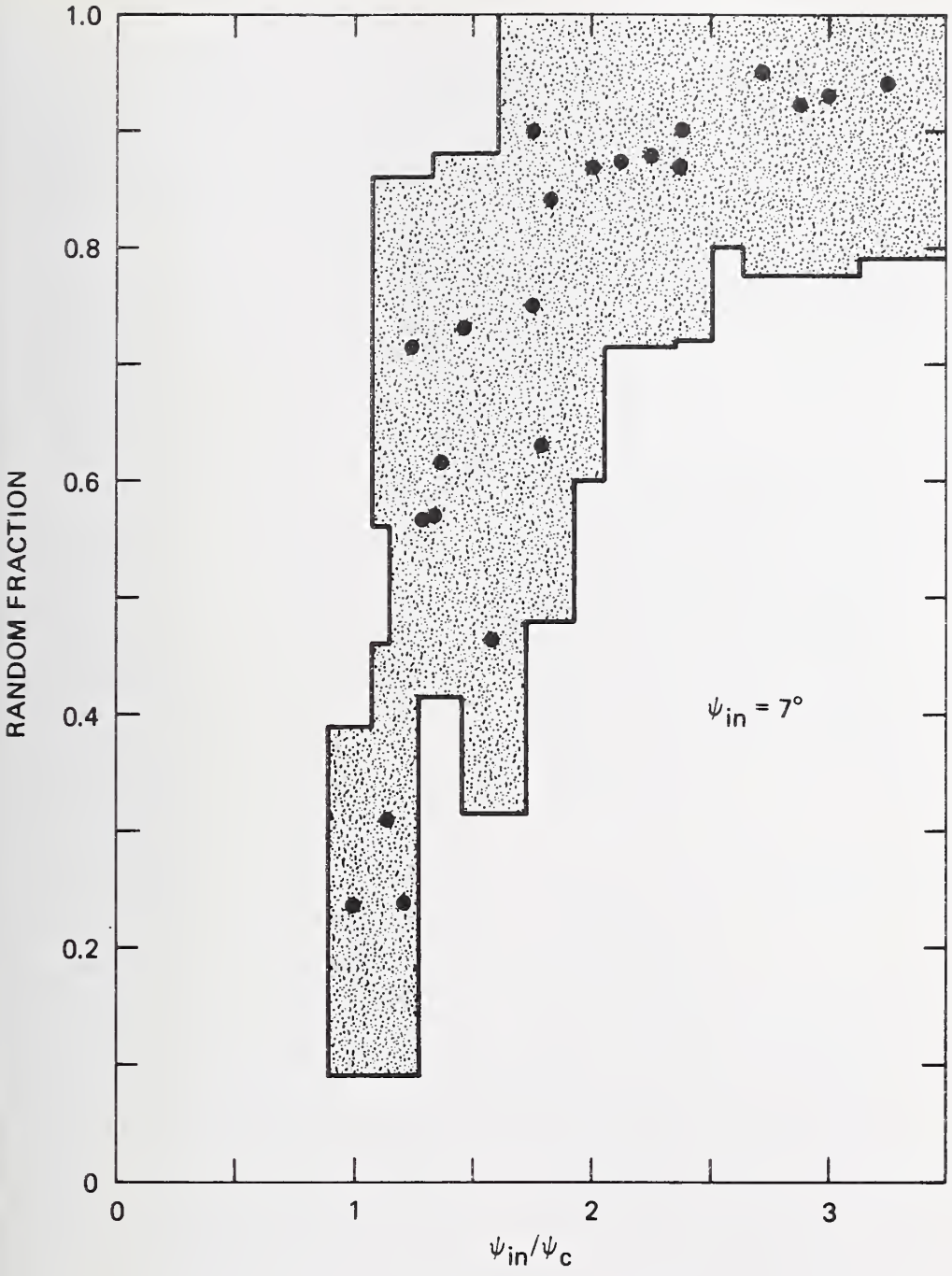


Figure 24a. Random fraction (linear) of implanted depth distributions versus the ratio of the selected random equivalent angle of incidence ($\psi_{in}$ = 7 deg) to the calculated critical channeling angle.

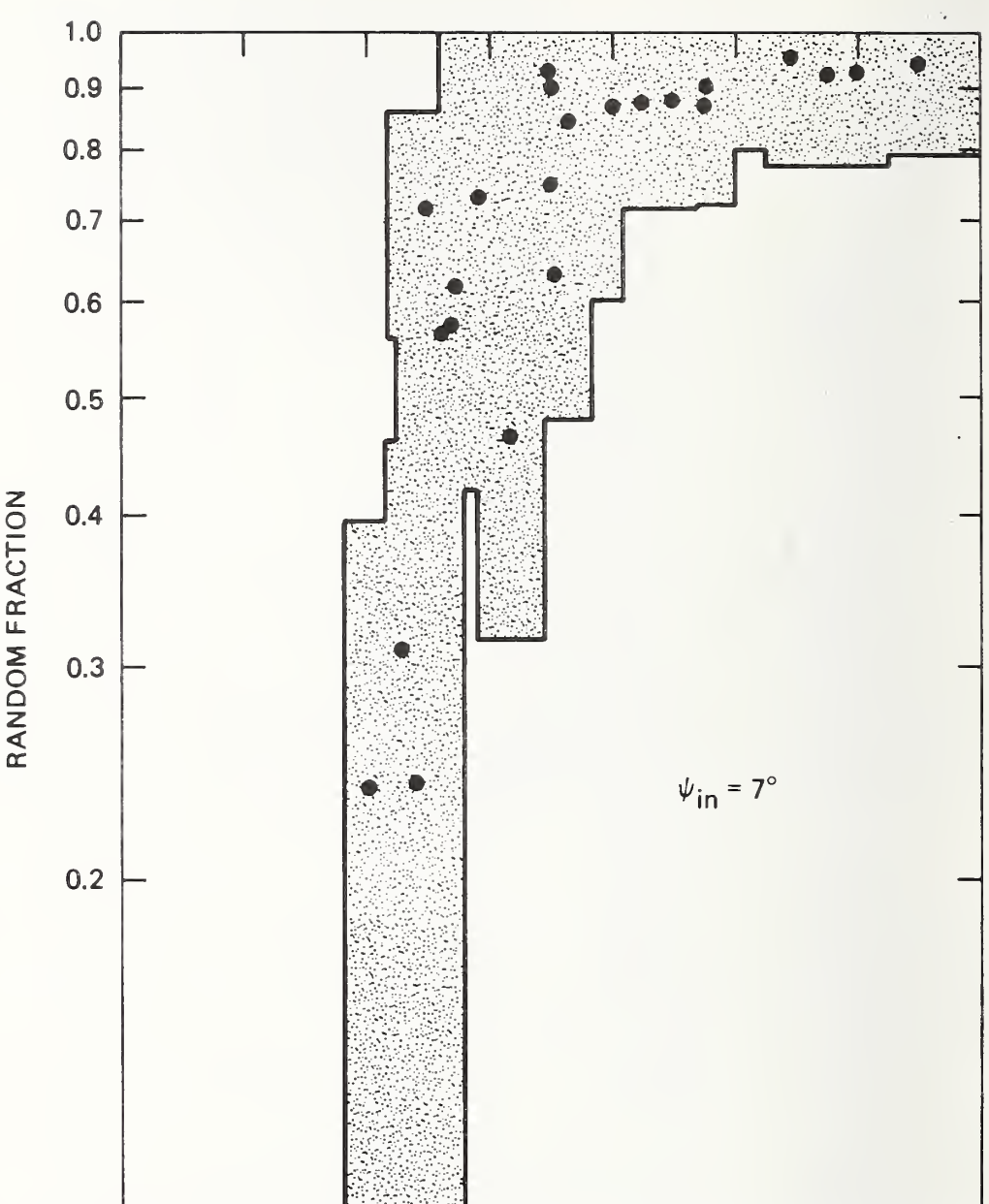


Figure 24b. Random fraction (log) of implanted depth distributions versus the ratio of the selected random equivalent angle of incidence ($\psi_{in}$ = 7 deg) to the calculated critical channeling angle.

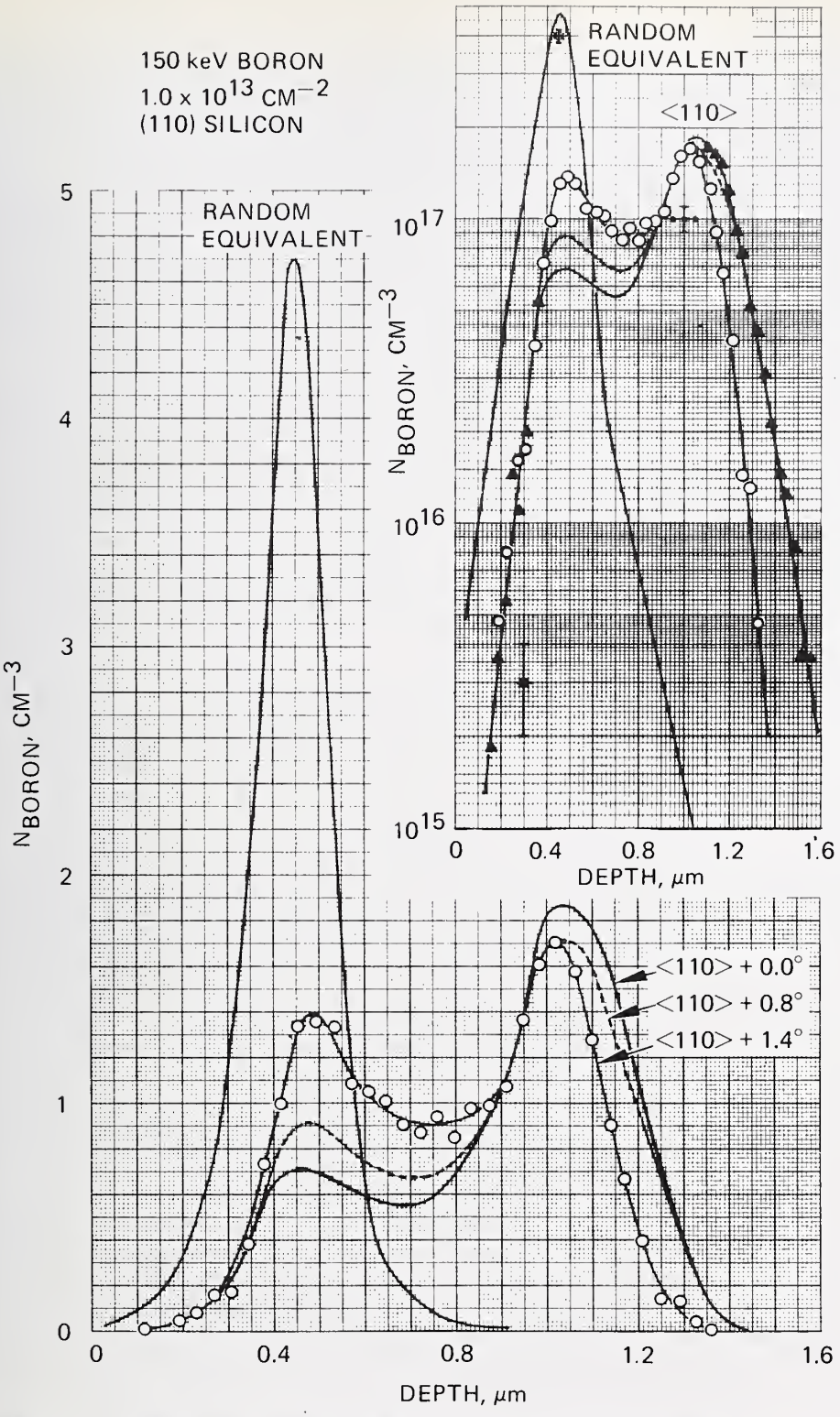


Figure 25. SIMS atom-depth distributions for 150-keV boron as a function of alignment angle away from the [110] axis of silicon. Solid curves are drawn through the individual data points from the SIMS measurement. Typical data points are represented by the circles and triangles.

sentative steps between optimum alignment and (110) random equivalent alignment. The SIMS data of figure 25 should be compared with the C-V data of figures 9 and 10, which are for ion energies a factor of two greater than and less than that used to obtain the SIMS energy. The shapes of the curves and the qualitative nature of the transition between alignment conditions are seen to be in good agreement. The quantitative differences can be explained by the fact that the sets of alignment angles for the SIMS profile and for the C-V measurements were made in different directions away from 0-deg alignment, that is, the angle $\theta$ was varied at different values of $\phi$ (see figs. 1 and 2).

The depths of the peaks in the carrier concentration profiles of figures 7 through 13 are seen to shift as the alignment angle is varied. In most of the cases examined in this study, the peak moves uniformly from the random peak toward the optimally channeled peak as the ion beam approaches a low index crystallographic direction. This behavior is clearly exhibited by the boron profiles of figures 7, 9, and 25. However, the arsenic profiles of figures 12 and 13 do not follow this trend. In those profiles, the near-surface peak first moves deeper as the alignment angle decreases from the random equivalent angle, then shifts rapidly back toward the surface to even shallower depths than the depth of the random equivalent peak. Eltekov *et al.* [9] have performed calculations which illustrate shifts in the peak of the dopant distribution, as described above. The physical reasons for this shift in the peak location are discussed in 4.4.3.

## 4. ANALYSIS

While satisfactory theories are available to predict ion ranges in amorphous targets, there are at present no such theories to predict ion distributions in single crystals. Thus, this section provides a physical picture of the channeling process based on the analytic model of Lindhard [10]. This model is of sufficient generality to provide a means to characterize a wide variety of implantation parameters and to explain trends in the data. Lindhard's model begins with the concept of a string of atoms, which leads to the classification of an ion's trajectory in a single crystal according to its "transverse energy", i.e., the component of the ion's energy in the plane perpendicular to the atomic string. Classification of the ion's trajectory according to transverse energy in turn leads to the concept of a critical angle. It is then shown that while the critical angle describes only the limit of applicability of the continuum model, this concept provides a useful means of characterizing the implantation conditions. Finally, the implications obtained from this model for implantation into single crystal substrates are explored.

### 4.1. The Continuum Model

The stopping of energetic ions in crystals is typically addressed as a problem in classical mechanics [11] in which the scattering of an ion from an atom initially at rest is described as the motion of the ion in the central field of the ion-atom potential. Typically, the ion-atom

combination is modeled by the Thomas-Fermi potential [11], because of its simplicity and generality. The use of this potential, combined with a velocity-dependent electronic stopping power, leads to LSS-type range equations for implantations into amorphous substrates. Solutions of these equations yield predictions of ion range distributions accurate to approximately 10 percent for ion range and approximately 30 percent in the standard deviation in the projected range of the implanted ions [8,12]. Solutions to the range equations have been compiled by a variety of authors (e.g., [8,12,13]), and are used to predict ion ranges for industrial implants. However, these models are based on the assumption that the substrate atoms are randomly distributed, and therefore by their nature cannot predict the effects of the ordered nature of the crystalline lattice that are responsible for channeling.

To model the channeling effect, Lindhard approximated the substrate lattice by a series of strings of atoms parallel to the low index crystalline directions. If V(r) is the potential energy between an isolated atom and the incident ion, then the potential of an ion due to an infinite string of atoms at an average spacing d along the z axis (fig. 26) is given by:

$$V_T = \sum_{n=-\infty}^{\infty} V(r_n) = \sum_{n=-\infty}^{\infty} V(\sqrt{\rho_n^2 + z_n^2}) = \sum_{n=-\infty}^{\infty} V(\sqrt{\rho_n^2 + n^2 d^2}) \quad . \qquad (1)$$

Lindhard then argued that since the ions are moving with high velocity, and since the collision angles are small for channeled trajectories, the channeled ion would interact with many atoms at once. For these ions, details of the atomic nature of the lattice would become blurred, so that the atomic distribution would appear uniform. Mathematically, this would imply the limit of a continuous string

$$V_T \rightarrow \frac{1}{d} \int_{-\infty}^{\infty} V\left[\left(\rho^2 + z^2\right)^{1/2}\right] dz \equiv U(\rho) \quad . \qquad (2)$$

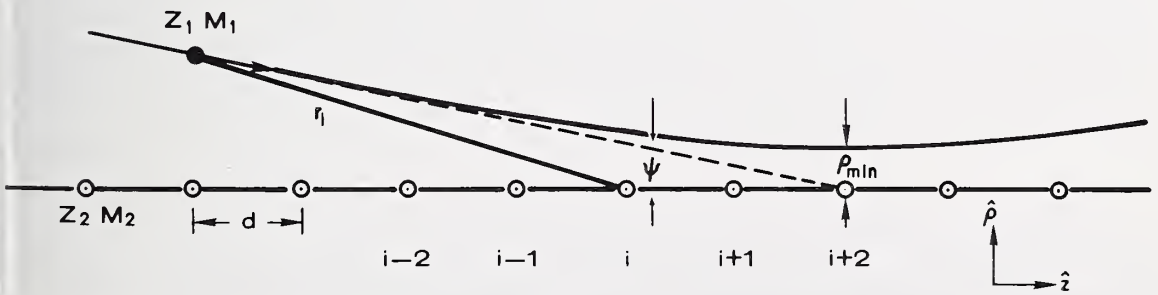


Figure 26. Illustration of symbols used to describe channeling parameters for an atomic string.

Using Lindhard's approximation to the Thomas-Fermi potential [9]:

$$V(r) = \frac{Z_1 Z_2 e^2}{4\pi\varepsilon_o r}\left[1 - \frac{r}{(r^2 + K^2 a^2)^{1/2}}\right], \tag{3}$$

the integral (2) becomes

$$U(\rho) = \frac{1}{d}\int_{-\infty}^{\infty} dz\, V\left[\left(z^2 + \rho^2\right)^{1/2}\right] = \frac{Z_1 Z_2 e^2}{4\pi\varepsilon_o d}\,\xi\,(\rho/a)\ , \tag{4}$$

where

$$\xi\,(\rho/a) = \ln\{(Ka/\rho)^2 + 1\}\ , \tag{5}$$

and

$$a = 0.8853\, a_B\,(Z_1^{2/3} + Z_2^{2/3})^{-1/2}\ . \tag{6}$$

In these expressions d is the average atomic spacing along the chosen crystallographic direction, r is the separation between the ion and the substrate atom, $Z_1$ is the atomic number of the ion, $Z_2$ is the atomic number of the substrate atom, $\varepsilon_o$ is the permittivity of vacuum ($8.854 \times 10^{-12}$ F/m), e the electronic charge ($1.602 \times 10^{-19}$ C), K is an adjustable constant, $\rho$ is the perpendicular distance from the ion to the string, and a is the Thomas-Fermi screening radius with $a_B$ being the Bohr radius (0.528 Å). Over a wide range of ion energies, the best fit to the potential $U(\rho)$ is obtained by setting $K = \sqrt{3}$ [10].

Since the potential energy now depends only on $\rho$ (the distance from the string), the only effective forces on the ion are normal to the row. This treatment neglects the contribution of electronic stopping which, since it is purely frictional, provides no directional effects. The model has thus reduced the classification of the ion's trajectory in a three-dimensional crystal to the problem of the motion of the ion in a plane perpendicular to the atomic string. Neglecting electronic stopping, the total energy of the ion in this transverse plane ($E_\perp$) is a constant, equal to the sum of the potential energy $U(\rho)$ plus the transverse kinetic energy $E_{K\perp}$. For an ion incident to the string at an angle $\psi$ with initial kinetic energy E given by

$$E = \frac{1}{2} M_1 v^2 \tag{7}$$

where $M_1$ is the mass of the ion and v is the incident velocity of the ion, the transverse kinetic energy is given by

$$E_{K\perp} = \frac{1}{2} M_1 (v\sin\psi)^2 \approx \frac{1}{2} M_1 v^2\psi^2 = E\psi^2\ . \tag{8}$$

(The approximation $\sin \psi \approx \psi$ is valid if $\psi$ is small.) The total transverse energy is given by

$$E_{\perp} = U(\rho) + E_{K\perp} = U(\rho) + E\psi^2 . \qquad (9)$$

## 4.2. Classification of Ion Trajectories

The continuum model leads to the understanding of channeled trajectories as characterized by the motion of an ion in a plane perpendicular to a single atomic string. The results obtained from this model are applied to trajectories in a real crystal by treating the crystal as a periodic arrangement of parallel strings. Thus, the potential energy for an ion entering the crystal is a sum of the potentials from each of the atomic strings. Because the crystal is periodic, only the potential in a single axial channel need be considered to understand the potential throughout the entire crystal. The ion-atom potential as given by eq (3) is a repulsive potential. Thus, the potential energy rises from a minimum value in the center of an axial channel to an infinite value as the ion approaches the center of any atomic string. It is important to note that in the region between the strings that form the boundary of the axial channel, the potential assumes an intermediate value — a higher potential energy than it has at the center of the channel, but lower than the potential energy very near the atomic strings.

The continuum model predicts three types of stable trajectories and a fourth (unstable) trajectory [14]. The three stable trajectories are illustrated in figure 27, looking down the atomic strings at the projection of the ion's motion in the plane perpendicular to the atomic strings.

The first type of ion motion is the perfectly channeled (or hyperchanneled) trajectory (fig. 27a). This trajectory occurs for ions that enter the crystal in a region of low potential energy with a very low transverse kinetic energy. Because of their low transverse energy, the motion of these ions is confined to a single axial channel. These are the ions that penetrate the deepest into the crystal and produce the "optimally channeled" distribution referred to in section 3. of this report.

Ions with somewhat higher values of transverse energy (fig. 27b) wander among the strings of atoms. While these ions have enough transverse energy to overcome the potential barrier that confines the perfectly channeled ions to a single axial channel, they do not have enough transverse energy to approach the string of atoms closely enough to see the atoms as individual scattering centers. The continuum model still describes the motion of this class of ions, which follow what is referred to as a "channeled" trajectory.

Ions with transverse energy greater than some critical value ($E_c$) approach the string of atoms closely enough to see the substrate atoms as individual scattering centers (fig. 27c). Transverse energy is no longer conserved, and the continuum model of the atomic string no longer holds. Since the orderly arrangement of lattice atoms plays no part in

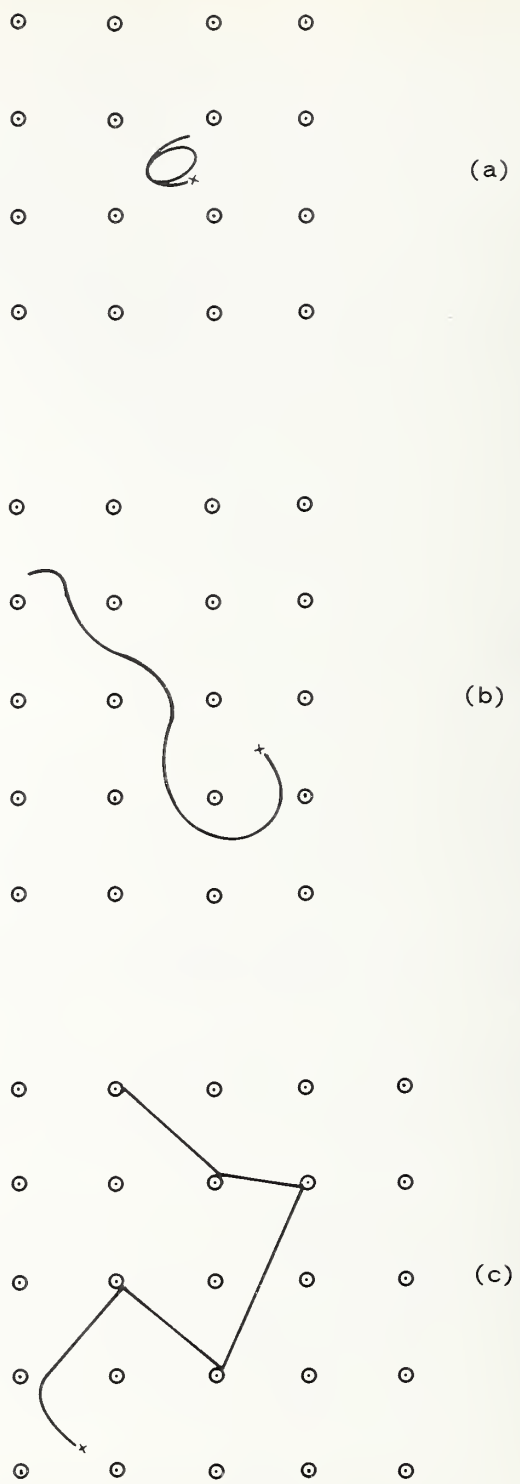


Figure 27. Hypothetical channeling trajectories in a simple cubic crystal (after [14]). Ions are incident with velocity component into the page.

influencing the trajectory of this last class of ions, the substrate atoms are randomly arranged in regard to the ion's motion. The distribution of the last type of ions should therefore be described by the range theories for amorphous targets.

Finally, there is a fourth type of unstable ion trajectory. This trajectory is followed by ions with transverse energies just above the critical energy. The motion of these "quasi-channeled" ions initially resembles a channeled trajectory; however, these ions have enough transverse energy to ultimately penetrate to the core of the atomic strings and thereby become deflected into a random trajectory. The number of deflections inside the channel an ion undergoes in this state before suffering a large angle scattering event is controlled entirely by chance [15]; however, while the ion is in this state, it spends much of its time in regions of the channel near the atomic strings. Thus, these ions see a greater elastic stopping power (typically 50 percent greater [15]) than for random trajectories, until such time as the ion becomes deflected into a random trajectory.

### 4.3. The Critical Angle

The continuum model does not describe the motion of ions with transverse energy above the critical value $E_c$. By eq (9) the transverse energy is a sum of a potential energy term and a kinetic energy term. Two concepts are related to that of a critical transverse energy, i.e., the critical approach distance and the critical angle. The critical approach distance ($\rho_c$) is the distance from an atomic string within which an ion can approach the string with zero transverse kinetic energy ($\psi = 0$) and can still exceed the critical energy. The critical angle ($\psi_c$) is the angle at which an ion can enter the crystal in a region of zero potential energy ($U = 0$) and have transverse kinetic energy equal to the critical energy. Thus,

$$E_c = E\psi_c^2 = U(\rho_c) \quad . \tag{10}$$

The ability to predict channeling behavior from the continuum model thus reduces to the problem of finding the critical approach distance ($\rho_c$) as a function of incident ion energy E. Fortunately, a solution to this problem has been given by Morgan and van Vliet [14], on the basis of computer modeling. They found that the minimum distance of approach to the string ($\rho_{min}$) is given by

$$\rho_{min} = \frac{2a\sqrt{\alpha}}{3}\left(1 - \frac{\sqrt{\alpha}}{19} + \frac{\alpha}{700}\right) \tag{11}$$

for $0.02 < \alpha < 350$, where a is defined in eq (6) and $\alpha$ is given by

$$\alpha = \frac{E'}{2E} \tag{12}$$

where

$$E' = \frac{2Z_1 Z_2 e^2 d}{4\pi\varepsilon_o a^2} \quad . \tag{13}$$

So far, channeling behavior has been estimated as if the lattice atoms were frozen in place; however, the real lattice is characterized by thermal vibrations. These vibrations are modeled in the Debye approximation [16] where the rms displacement ($u_{rms}$) of the lattice atoms from their equilibrium potential is given by

$$u_{rms} = 12.1 \{[\phi(\theta/T)/(\theta/T) + 1/4]/M_2\theta\}^{1/2} \text{ Å} \tag{14}$$

where $M_2$ is the atomic mass of the substrate (28.086 for silicon), $\theta$ is the Debye temperature (543 K for silicon), T is the absolute temperature, and $\phi(\theta/T)$ is the Debye function (tabulated in Abramowitz and Stegun [17]). The value of $u_{rms}$ for silicon at 293 K is 0.075 Å.

In the presence of thermal vibrations, the critical approach distance is given by [15]:

$$\rho_c^2 = \rho_{min}^2 + u_{rms}^2 \quad . \tag{15}$$

It can be seen from the form of eq (11) that at high ion energies the critical approach distance is limited by the thermal vibrations of the lattice, while at low ion energies, the critical approach distance is limited by the nature of the ion-atom potential. Finally, the critical angle can be calculated from eq (10) by substituting $\rho_c$ from eq (15) into the expression for string potential (eq (4)):

$$\psi_c = \sqrt{U(\rho_c)/E} \quad . \tag{16}$$

The above approach is valid over a range of incident energies characterized by a range of $\alpha$ from 0.02 to 350. In the case of very high implantation energies ($\alpha < 0.02$) the computer fit to $\rho_{min}/\alpha$ is no longer appropriate, so that Lindhard [10] calculates the critical angle from

$$\psi_c = \psi_1 = \left(\frac{2Z_1 Z_2 e^2}{4\pi\varepsilon_o dE}\right)^{1/2} \tag{17}$$

In the low energy limit ($\alpha > 350$), the computer fit again is no longer appropriate, and Lindhard calculates the critical angle from

$$\psi_c = \psi_2 = (\sqrt{3/2}\ a/d\ \psi_1)^{1/2} \quad . \tag{18}$$

Lindhard obtained eqs (17) and (18) by analyzing the asymptotic behavior of $U(\rho)$ in the high energy and the low energy limits, respectively [10]. The procedure for calculating the critical angle is summarized in Appendix A.

## 4.4. Implications for Implantations into Single Crystalline Substrates

### 4.4.1. Physical Interpretation of the Critical Angle

The critical angle as calculated above describes only the limit of applicability of the model used and not the angular extent of channeling behavior. Experience obtained from channeling experiments on a variety of ion-target combinations indicates that the critical angle corresponds very closely to the angle at which the random fraction is halfway between the value for 0-deg beam incidence and the saturation random value. This latter angle is referred to as $\psi_{1/2}$, and the experience obtained to date [14] indicates that

$$\psi_{1/2} = k\psi_c \tag{19}$$

with

$$k = 0.8 - 1.0 \quad . \tag{20}$$

Both experimental studies and computer simulations indicate that channeling characteristics persist until the angle of incidence for the beam is at least twice the classical critical angle away from the nearest low index crystalline direction [15], as also is seen in the work reported here for ions and energies characteristic of industrial implantation conditions.

### 4.4.2. Crystal Orientation for Minimal Channeling

From the data presented and from the previous discussion, it is seen that the substrate must be tilted so that the nearest low index crystalline direction is twice the calculated critical angle away from the beam direction to minimize the extent of ion channeling. This angle can exceed the 7- or 8-deg tilt commonly used for randomization in implantation today, especially for implants made at low energy or high atomic number. Examination of table 1 indicates that for the ions studied here, the critical angle varies from 1.97 deg to 6.86 deg, requiring tilt angles of from at least 4 deg to almost 14 deg for maximum random yield. When $2\ \psi_c$ exceeds the commonly employed random equivalent tilt angle for (111)-oriented silicon of 7- to 10-deg, care should be given to whether the use of the larger angle may cause another planar or axial channeling condition to be approached within $2\ \psi_c$ (see fig. 2 for an illustration).

In addition to predicting the angle needed to maximize the random yield (i.e., twice $\psi_c$), the continuum model describes additional useful trends in the data. As was discussed in 4.3., a circle of radius $\rho_c$ around each atomic string describes the area in which an ion entering even at 0-deg incidence will follow a random trajectory. For ions uniformly distributed about the entire crystal surface, an estimate of the random fraction for 0-deg incidence can be obtained by multiplying the area within $\rho_c$ of the string ($\pi\rho_c^2$) by the number of strings per unit area [15]. Thus, the random fraction for 0-deg incidence R.F. (0) is given by

$$\text{R.F. (0)} = \pi\rho_c^2 \, Nd \ , \tag{21}$$

where Nd is the number of strings per unit surface area: N is the atomic density of the target ($4.866 \times 10^{22}$ $cm^{-3}$ for silicon) and d is the average atomic spacing along the string. Since the critical approach distance increases as the critical angle increases (eq (11)), the continuum model explains an apparent paradox: that as the angular requirements for channeling to occur become less restrictive (i.e., as $\psi_c$ increases), the fraction of ions that never become channeled increases (due to the increase in $\rho_c$). Thus, performing a given implantation at a lower energy may or may not increase the channeled fraction, depending on the ion and substrate orientation chosen.

### 4.4.3. Effects of Channeling on Ion Distributions

In 4.2. of this report, four different types of ion trajectories, each with its own directional effects and stopping power, were described. At present, the final depth distribution of implanted ions in general can be predicted for only one of the four components of the ion beam, namely, for those ions that follow a random trajectory on entering the crystal. As a result, one must exercise great caution in applying the range theory developed for amorphous targets to predict the results of implantations into single-crystal targets. It is impossible at present to predict the ion range distribution in single-crystal targets without extensive computer modeling for each set of implantation conditions, as was done for the case of 200-keV boron implanted into (111)-oriented silicon in [9]. Physically, as the angle of beam incidence is changed, the transverse kinetic energy of the incident ions also is changed. This alters the relative fraction of ions that follow each type of trajectory (since the type of trajectory an ion follows is determined by its transverse energy); however, the details of each trajectory and the relative magnitudes of each of the beam components depend in an intricate manner on the details of the ion-substrate potential. Thus, many features of the final range distribution cannot be predicted on the basis of intuition. An example of this can be found in the present experimental results by considering the location of the near-surface peak in the distribution of electrical activity as a function of alignment angle (figs. 7 through 13). Only when the angle of incidence is approximately twice the critical angle does the location of the near-surface peak coincide with that predicted by the range theory for amorphous targets. Peaks that occur

deeper than the random peak indicate that the channeled component of the beam, with its reduced stopping power, is dominating the formation of the ultimate depth distribution of the implanted ions. Peaks that occur closer to the surface than the random peak (such as is seen in the arsenic profiles of figs. 12 and 13) indicate the importance of the quasi-channeled component with its greatly increased stopping power. Until adequate theoretical models can be developed, empirical profiles are the only guide toward understanding the physical phenomena.

### 4.4.4. Effect of Amorphous Surface Layers

It must be noted that the theory that has been explained in this report applies to the case of implantation directly into the surface of a single crystal. This development specifically neglects consideration of the effect of amorphous surface layers (such as $SiO_2$, $Si_3N_4$, or unannealed previous high-fluence implantations) on the extent of ion channeling. The reduction of ion channeling for a crystalline substrate perfectly oriented to the ion beam direction but covered by an amorphous surface layer can be estimated by analytic procedures [18]. These expressions do not consider the effect of substrate tilt on the extent of ion channeling for the composite structure. Furthermore, these expressions have been experimentally examined only for high energy hydrogen or helium backscattering and have not been tested for heavy ion implantation.

## 5. INFLUENCE OF SCANNING

If it is desired to achieve uniform device characteristics everywhere over a 5- to 10-cm diameter silicon wafer using either intended random equivalent or well channeled implants, the data reported in the preceding sections of this report show that the angle of incidence of the ions must be controlled everywhere over the wafer to guarantee controlled depth profiles. In this section, industrial production implantation target chamber/beam scanning techniques are considered, and the application of the results presented in this report to industry practice is discussed.

Uniform implantation of large wafers requires some method for scanning the ion beam across the wafers or of scanning the wafers in a stationary beam. Some of the techniques presently in use can result in angular variations across the surface of a wafer or from wafer to wafer that can create significant variations in depth distribution and therefore can cause loss of control of junction depth or device characteristics, resulting in poor yield. Other scanning techniques maintain a constant angle of incidence, but that angle may not be the angle required. In such cases, channeling may occur and may cause junctions or distributions to be deeper than were designed using LSS range statistics.

There are two general techniques for scanning, namely, electrostatic beam scanning and mechanical target scanning. Ion beam scanning techniques are discussed by Wittkower [19], Wilson and Brewer [20], and Dearnaley, Freeman, Nelson, and Stephen [21]. Sometimes the two are combined, one

in each dimension. Two types of each scanning technique will be considered to establish criteria that can be applied to other techniques. As ion beam currents are increased in advanced implantation systems, mechanically scanned target systems are favored, because 1) electrostatic scanning removes the space-charge neutralizing electrons from the ion beam which results in expansion of the beam, and 2) of the need to distribute the input power over a number of wafers to reduce heating effects Crystalline wafers of 75-mm diameter oriented to within about 1 deg of a low index plane after polishing are assumed in the following discussion.

### 5.1. Mechanical Target Scanning (Ion Beam Fixed)

#### Case A

SCAN: Wafers are mounted on a disk that rotates about an axis parallel to the ion beam and translates linearly from side to side in a plane normal to the ion beam. In another version, the target mount is translated linearly in two directions in a plane normal to the ion beam.

ANGULAR CONDITION: The angle is constant for all wafer surfaces, so angular uniformity is good everywhere; but the angle between the ion beam and the wafer orientation is near 0 deg so channeling can be significant.

DISCUSSION: For nominal channeling, this condition is ideal. If random equivalent depth distributions are desired, the axis of rotation should be tilted at twice the critical angle from the direction of the ion beam.

#### Case B

SCAN: The wafers are mounted on the surface of a cylinder which is rotated about an axis normal to the ion beam and is translated along the axis of rotation (or the ion beam is scanned in one dimension).

ANGULAR CONDITION: The angle of incidence between the ions and the wafer crystallographic axes varies over each wafer surface from 0 deg to ∿7 to 9 deg, depending on the diameter of the cylinder, so the perfect channeling condition may occur in one location on the wafer and the random equivalent in another. There is no angular control.

DISCUSSION: Angular control is not possible if the cylinder surface is normal to the ion beam direction. If the cylinder facets are wedged or machined at twice $\psi_c$, then implants for minimal channeling can be achieved.

### 5.2. Electrostatic Beam Scanning (Wafers Fixed)

#### Case A

SCAN: The ion beam is scanned in two dimensions to cover one wafer mounted on a surface normal to the beam or tilted 7 deg from the normal, and the wafers are sequenced into the beam scan area.

ANGULAR CONDITION: The angle of incidence typically varies ∿1 to 2 deg over a wafer surface, and therefore channeling cannot be controlled. This condition is probably adequate to achieve uniform random equivalent implants if the wafer surface is tilted 2 $\psi_c$ from the normal.

DISCUSSION: Nominal channeling cannot be achieved. No modifications are required for random equivalent implants.

Case B

SCAN: Double deflection scanning is used, which is the same as for Case A except that the beam is deflected a second time to make it parallel to the beam axis.

ANGULAR CONDITION: The angle is everywhere properly controlled for the random equivalent condition if the wafer plane is tilted at twice $\psi_c$. If the wafer plane is normal to the beam, then the angle is everywhere proper for nominal channeling.

DISCUSSION: If the proper angular alignment is achieved, no modifications are required for nominal channeling or random equivalent.

If $\psi_c$ is small enough to require accurate alignment to achieve channeling, then a goniometer and a simple Rutherford backscattering alignment system is required to produce well channeled implants for the parallel beam scanning or double deflection approach. The samples must be implanted individually in this case and implantation times will increase significantly. Accurate channeling alignment cannot be achieved when a number of wafers are mounted on one surface and implanted together as in the mechanical scanning techniques unless each wafer is polished to within ∿0.1 deg of the same orientation.

## REFERENCES


1. Andersen, J. U., Davies, J. A., Nielsen, K. O., and Andersen, S. L., An Experimental Study of the Orientation of (p,γ) Yields in Monocrystalline Aluminum, *Nucl. Instrum. Methods* 38, 210-215 (1965).

2. Seidel, T. E., Distribution of Boron Implanted Silicon, *Proc. Second International Conference on Ion Implantation in Semiconductors*, Garmisch-Partenkirchen, May 24-28, 1971, pp. 47-57 (Springer-Verlag, Berlin, 1971).

3. Moline, R. A., Ion Implanted Phosphorus in Silicon: Profiles Using C-V Analysis, *J. Appl. Phys.* 42, 3553-3558 (1971).

4. Moline, R. A., and Reutlinger, G. W., Phosphorus Channeled in Silicon: Profiles and Electrical Activity, *Proc. Second International Conference on Ion Implantation in Semiconductors*, Garmisch-Partenkirchen, May 24-28, 1971, pp. 58-69 (Springer-Verlag, Berlin, 1971).

5. Reddi, V. G. K., and Sansbury, J. D., Channeling and Dechanneling of Ion-Implanted Phosphorus in Silicon, *J. Appl. Phys.* 44, 2951-2963 (1973).

6. Gordon, B. J., Stover, H. L., and Harp, R. S., A New Impurity Profile Plotter for Epitaxy and Devices, *Silicon Device Processing*, C. P. Marsden, Ed, NBS Special Publication 337, pp. 273-284 (November 1970).

7. Kennedy, D. P., Murley, P. C., and Kleinfelder, W., On the Measurement of Impurity Atom Distributions in Silicon by the Differential Capacitance Technique, *IBM J. Res. Development*, September 1968, pp. 399-408; and Kennedy, D. P., and O'Brien, R. R., On the Measurement of Impurity Atom Distributions in Silicon by the Differential Capacitance Technique, *IBM J. Res. Development*, March 1969, pp. 212-214.

8. Brice, D. K., Spatial Distribution of Ions Incident on a Solid Target as a Function of Instantaneous Energy, Sandia Labs Report SC-PR-71-0599, Albuquerque, New Mexico (1971), and *Appl. Phys. Lett.* 16, 103-106 (1970).

9. Eltekov, V. A., Karpuzov, D. S., Martynenko, Y. V., Rubakha, E. A., Simonov, V. A., and Yurasova, V. E., Computer Studies of Boron Ion Channeling in Silicon Single Crystals, *Proc. International Conference on Atomic Collisions in Solids (IV)*, 1971, S. Andersen, K. Björkqvist, B. Domeij, and N. G. E. Johansson, Eds., (Gordon and Breach, London, 1972), pp. 113-118.

10. Lindhard, J., Influence of Crystal Lattice on Motion of Energetic Charged Particles, *Kgl. Danske Videnskab. Selskab, Mat.-Fys. Medd.* 34 (14) (1965).

11. Sigmund, P., Collision Theory of Displacement Damage, *Rev. Roum. Phys.* 17, 823-870, 969-1000, and 1070-1106 (1972).

12. Gibbons, J. F., Johnson, W. S., and Mylorie, S. W., *Projected Range Statistics - Semiconductors and Related Materials*, 2nd ed., (Stroudsburg, Dowden, Hutchinson and Ross, 1975).

13. Winterbon, K. B., *Ion Implantation Range and Energy Deposition Distributions* 2 (Plenum, New York, 1975).

14. Morgan, D. V., and Van Vliet, D., Critical Approach Distances and Critical Angles for Channeling; *Radiat. Eff.* 8, 51-61 (1971).

15. Van Vliet, D., The Continuum Model of Directional Effects, *Channeling, Theory Observation and Applications*, D. V. Morgan, Ed (Wiley, New York, 1973).

16. See, for example, Gemmell, D. S., Channeling and Related Effects in the Motion of Charged Particles Through Crystals, *Rev. Mod. Phys.* 46, 129-227 (1974).

17. Stegun, I. A., Miscellaneous Functions: Debye Function, in Handbook of Mathematical Functions for Formulas, Graphs, and Mathematical Tables, M. Abramowitz and I. A. Stegun, Eds, *Nat. Bur. Stand., Appl. Math. Ser.* 55 (June 1964), p. 998.

18. Lugujjo, E., and Mayer, J. W., Energy Dependence of $He^+$ and $H^+$ Channeling in Si Overlaid with Au Films, *Phys. Rev. B.* 7, 1782-1791 (1973).

19. Wittkower, A., Wafer Handling for Ion Implantation, *Electronic Packaging and Production*, 95-104 (May 1973).

20. Wilson, R. G., and Brewer, G. R., *Ion Beams*, p. 457 (Wiley-Interscience Publishers, New York, 1973).

21. Dearnaley, G., Freeman, J. H., Nelson, R. S., and Stephen, J., *Ion Implantation* (North Holland Publishing Company, Amsterdam, 1973).

## APPENDIX A. CALCULATION OF THE CRITICAL ANGLE

In this report, it has been demonstrated that the crystals must be oriented at twice the classical critical angle to minimize unintentional channeling. This appendix provides an outline of the procedure used to calculate the critical angle for implantations into silicon. The procedure is outlined as a series of steps.

STEP 1: Calculate a:

$$a = 0.8853\ a_B\ (Z_1^{2/3} + Z_2^{2/3})^{-1/2}$$

or

$$a = 0.4685\ (Z_1^{2/3} + 14^{2/3})^{-1/2}\ \text{Å} \tag{A1}$$

STEP 2: Using the proper value of atomic spacing from table A1, calculate $E^1$:

$$E' = \frac{2Z_1 Z_2 e^2 d}{4\pi\varepsilon_o a^2}$$

or

$$E' = 403.2\ \frac{Z_1 d}{a^2}\ \text{eV-Å} \tag{A2}$$

STEP 3: Calculate $\alpha$ for the implantation energy E chosen (the implantation energy E is the product of the accelerating voltage times the charge state of the ion, e.g., E = 400 keV for $B^{++}$ at 200 kV):

$$\alpha = \frac{E'}{2E} \tag{A3}$$

STEP 4: If $0.02 < \alpha < 350$

$$\rho_{min} = \frac{2a}{3}\sqrt{\alpha}\ \left(1 - \frac{\sqrt{\alpha}}{19} + \frac{\alpha}{700}\right) \tag{A4}$$

If $\alpha < 0.02$ Go to step 9.

If $\alpha > 350$ Go to step 10.

STEP 5: Calculate $u_{rms}$ for the implantation temperature using $M_2, \theta$ from table A1:

$$u_{rms} = 12.1\ \{[\Phi(x)/x + 1/4]/M_2\theta\} \tag{A5}$$

Table A1. Physical Constants for Silicon

| Quantity | Value for Silicon |
|---|---|
| $Z_2$ | 14 |
| $M_2$ | 28.086 amu |
| $d_{100}$ | 5.431 Å |
| $d_{110}$ | 3.840 Å |
| $d_{111}$ | 4.703 Å |
| $u_{rms}$ at 293°K | 0.075 Å |
| N | $4.995 \times 10^{-2}$ $(Å)^{-3}$ |
| $\theta$ | 543 K |

Table A2. Atomic Numbers ($Z_1$) For Commonly Implanted Impurities

| | |
|---|---|
| B | 5 |
| Al | 13 |
| P | 15 |
| Ga | 31 |
| As | 33 |
| In | 49 |
| Sb | 51 |

where

$$x = \frac{\theta}{T}$$

For room temperature implants into silicon:

$$u_{rms} \text{ at } 293 \text{ K} = 0.075 \text{ Å}$$

STEP 6: Calculate $\rho_c$

$$\rho_c = \sqrt{\rho_{min}^2 + u_{rms}^2} \tag{A6}$$

STEP 7: Calculate $U(\rho_c)$

$$U(\rho_c) = \frac{Z_1 Z_2 e^2}{4\pi\varepsilon_o d} \ln \left\{ \left(\frac{Ka}{\rho_c}\right)^2 + 1 \right\}$$

$$U(\rho_c) = 201.6 \frac{Z_1}{d} \ln \left\{ 3 \left(\frac{a}{\rho_c}\right)^2 + 1 \right\} \tag{A7}$$

STEP 8: Calculate $\psi_c$

$$\psi_c = \sqrt{\frac{U(\rho_c)}{E}} \tag{A8}$$

When $\alpha$ is not between 0.02 and 350, steps 9 and 10 replace steps 5 through 8.

STEP 9: If $\alpha < 0.02$

$$\psi_c = \psi_1 = \frac{a}{d} \left(\frac{E'}{E}\right)^{1/2} \tag{A9}$$

STEP 10: If $\alpha > 350$, calculate $\psi_1$ from step 9. Then

$$\psi_c = \psi_2 = \left(\sqrt{\frac{3}{2}} \frac{a}{d} \psi_1\right)^{1/2} \tag{A10}$$

## Sample Calculation

100 keV $As^+$ implanted into <100> oriented silicon at room temperature:

STEP 1: From equation (A1):

$$a = 0.4685\ (33^{2/3} + 14^{2/3})^{-1/2}\ \text{Å}$$

$$a = 0.1165\ \text{Å}$$

STEP 2: From equation (A2):

$$E' = 403.2\ \frac{(5.431\ \text{Å})\ (33)}{(0.1165\ \text{Å})^2}$$

$$E' = 5.324 \times 10^6\ \text{eV}$$

STEP 3: From equation (A3):

$$E = (1)\ (1 \times 10^5\ \text{eV}) = 10^5\ \text{eV}$$

$$\alpha = \frac{5.324 \times 10^6\ \text{eV}}{2(10^5\ \text{eV})} = 26.62$$

STEP 4: From equation (A4):

$$\rho_{min} = \frac{2(0.1165\ \text{A})}{3}\ \sqrt{26.62}\left(1 - \frac{\sqrt{26.62}}{19} + \frac{26.62}{700}\right)$$

$$\rho_{min} = 0.307\ \text{Å}$$

STEP 5: At room temperature $u_{rms} = 0.075$ Å.

STEP 6: From equation (A6):

$$\rho_c = \sqrt{(0.3071\ \text{Å})^2 + (0.075\ \text{Å})^2}$$

$$\rho_c = 0.3162\ \text{Å}$$

STEP 7: From equation (A7):

$$U(\rho_c) = 201.6\ \frac{33}{5.431\ \text{Å}}\ \ln\left\{3\left(\frac{0.1165\ \text{Å}}{0.3162\ \text{Å}}\right)^2 + 1\right\}$$

$$U(\rho_c) = 418.5\ \text{eV}$$

STEP 8: From equation (A8):

$$\psi_c = \sqrt{\frac{418.5 \text{ eV}}{10^5 \text{ eV}}} = 0.0647 \text{ rad}$$

$$\psi_c = 3.71 \text{ degrees.}$$

## APPENDIX B. DATA FROM THE LITERATURE

Two figures were constructed from data given in the literature for use in this work. They are shown below as figures B-1 and B-2. The source and explanations are given in the figure captions.

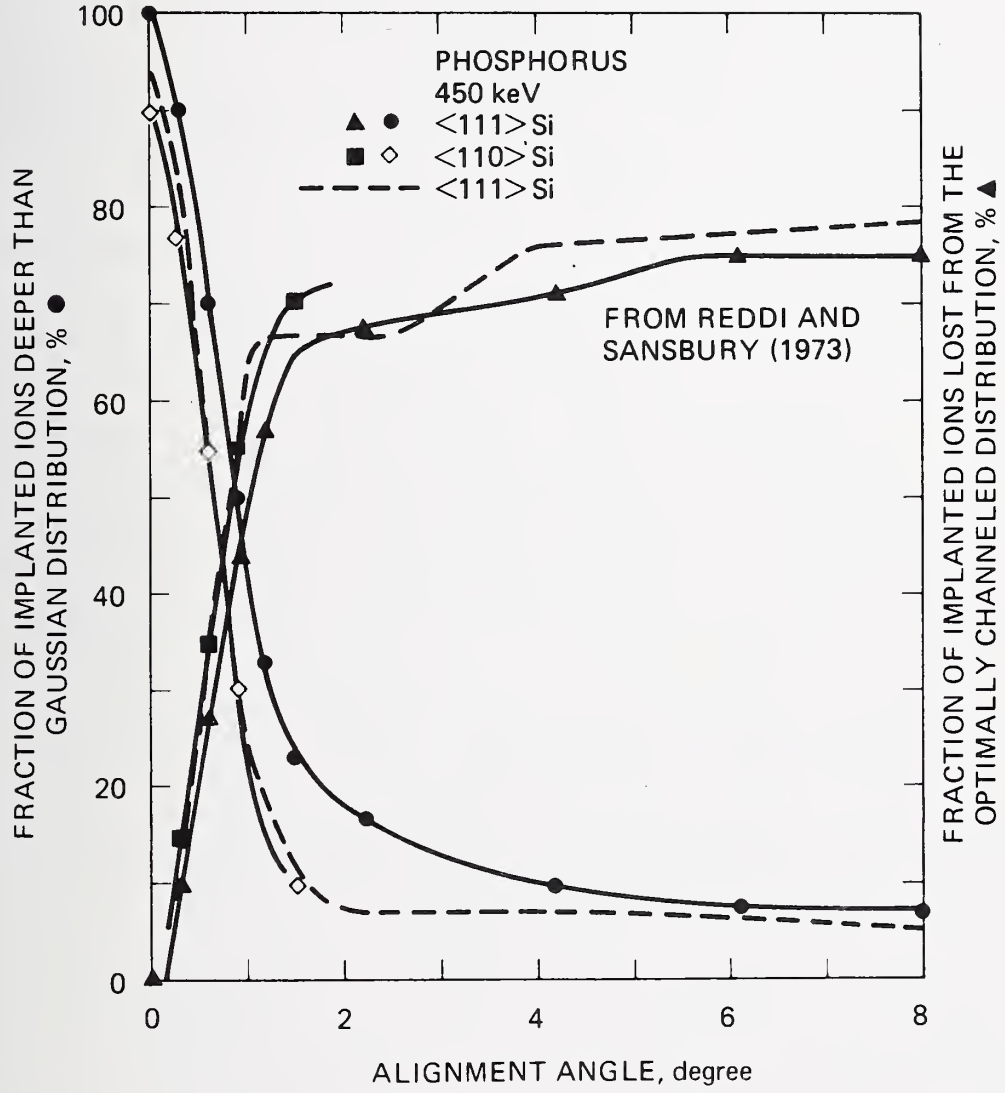


Figure B-1. Sensitivity of implanted depth distribution to implantation angle for 450-keV phosphorus in <111>, <110>, and <100> silicon. Data obtained from an analysis of curves published by Reddi and Sansbury [5].

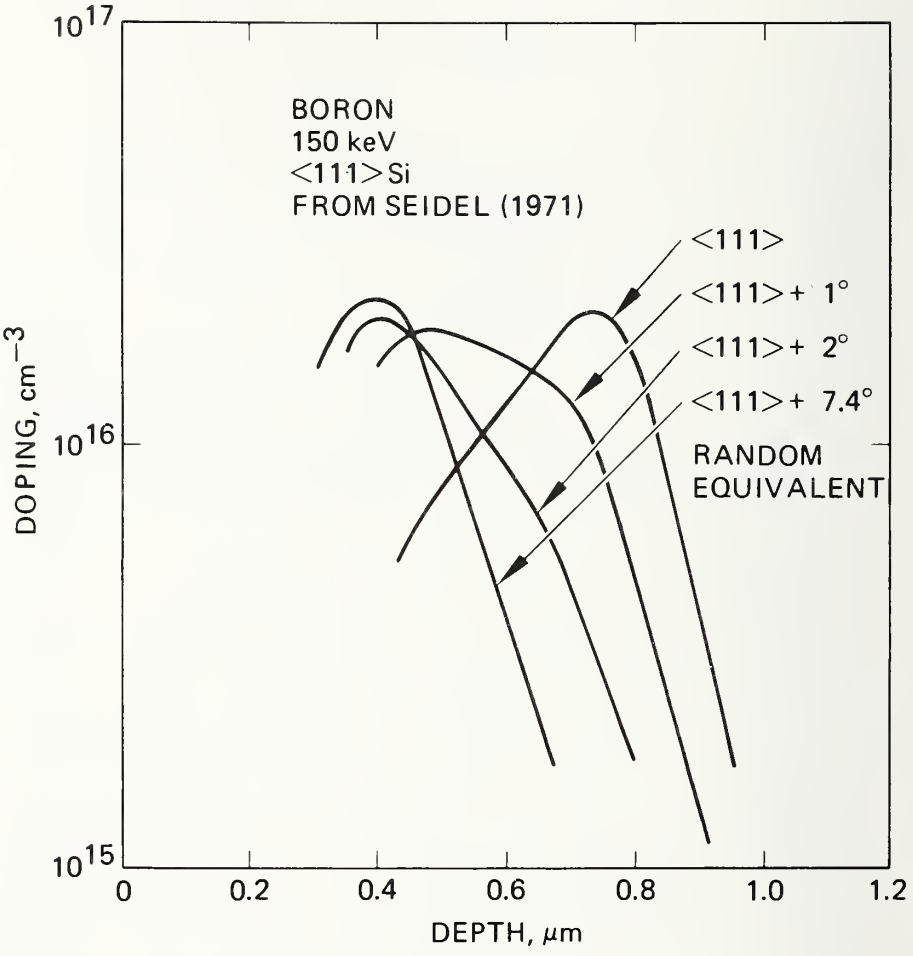


Figure B-2. Implanted depth distributions for 150-keV boron in <111> silicon from Seidel [2].

NBS-114A (REV. 11-77)

| U.S. DEPT. OF COMM. BIBLIOGRAPHIC DATA SHEET | 1. PUBLICATION OR REPORT NO. SP 400-49 | 2. Gov't Accession No. | 3. Recipient's Accession No. |
|---|---|---|---|

4. TITLE AND SUBTITLE

*Semiconductor Measurement Technology:* Angular Sensitivity of Controlled Implanted Doping Profiles

5. Publication Date: November 1978

6. Performing Organization Code


7. AUTHOR(S) Robert G. Wilson, Howard L. Dunlap, Douglas M. Jamba, and David R. Myers

8. Performing Organ. Report No.

9. PERFORMING ORGANIZATION NAME AND ADDRESS

Hughes Research Laboratories
3011 Malibu Canyon Road
Malibu, CA 90265

NATIONAL BUREAU OF STANDARDS
DEPARTMENT OF COMMERCE
WASHINGTON, D.C. 20234


10. Project/Task/Work Unit No.

11. Contract/Grant No. ARPA Order No. 2397
Program Code 6D10

12. Sponsoring Organization Name and Complete Address *(Street, City, State, ZIP)*

ARPA - 1400 Wilson Boulevard, Arlington, VA 22209

The National Bureau of Standards

13. Type of Report & Period Covered: Final

14. Sponsoring Agency Code

15. SUPPLEMENTARY NOTES

Library of Congress Catalog Card Number: 78-10624


16. ABSTRACT *(A 200-word or less factual summary of most significant information. If document includes a significant bibliography or literature survey, mention it here.)*

Ion implantation can be used to produce accurately controlled doping profiles for silicon devices and integrated circuits. The work reported here determines the angle at which the ion beam must strike the substrate in order to maintain control over the channeled and random equivalent depth distributions of carriers as measured by 1-MHz differential capacitance-voltage (C-V) profiling. A method to calculate the classical critical angle for channeling ($\psi_c$) is presented. Data are presented that characterize the variation in the depth distribution of carriers with substrate orientation, incident ion species, and incident ion energy, for a range of critical angles. This study establishes the degree of control of the angle between the ion beam and the crystallographic orientation needed to produce the limiting cases of either optimal channeling or maximum randomization of ion trajectory in the substrate. For the cases studied here, the angle between the ion beam and the substrate orientation must be controlled to within 0.5 ± 0.2 deg to obtain the optimally channeled depth distribution for implantation directly into the low index crystallographic orientations. Alternatively, to minimize unintentional channeling, the substrate must be oriented so that the nearest low index crystallographic direction is at least twice the classical critical angle away from the beam direction. The substrate tilt angles required to satisfy these conditions can exceed the 7- to 10-deg tilt commonly used in ion implantation. The implications of these results for uniform and reproducible ion implantation within the semiconductor industry are discussed.



17. KEY WORDS *(six to twelve entries; alphabetical order, capitalize only the first letter of the first key word unless a proper name; separated by semicolons)*

C-V profiling; controlled doping profiles; critical channeling angle; ion beam scanning; ion channeling; ion implantation; Rutherford backscattering alignment; silicon crystallographic orientation.


18. AVAILABILITY

[X] Unlimited

[ ] For Official Distribution. Do Not Release to NTIS

[X] Order From Sup. of Doc., U.S. Government Printing Office Washington, D.C. 20402, SD Stock No. SN003-003-

[X] Order From National Technical Information Service (NTIS) Springfield, Virginia 22151

| 19. SECURITY CLASS (THIS REPORT) | 21. NO. OF PAGES |
|---|---|
| UNCLASSIFIED | 61 |
| **20. SECURITY CLASS (THIS PAGE)** | **22. Price** |
| UNCLASSIFIED | $2.50 |

USCOMM-DC 66038 P78


☆ U.S. GOVERNMENT PRINTING OFFICE: 1978— 281-067/307

# NBS TECHNICAL PUBLICATIONS

## PERIODICALS

JOURNAL OF RESEARCH—The Journal of Research of the National Bureau of Standards reports NBS research and development in those disciplines of the physical and engineering sciences in which the Bureau is active. These include physics, chemistry, engineering, mathematics, and computer sciences. Papers cover a broad range of subjects, with major emphasis on measurement methodology, and the basic technology underlying standardization. Also included from time to time are survey articles on topics closely related to the Bureau's technical and scientific programs. As a special service to subscribers each issue contains complete citations to all recent NBS publications in NBS and non-NBS media. Issued six times a year. Annual subscription: domestic $17.00; foreign $21.25. Single copy, $3.00 domestic; $3.75 foreign.

Note: The Journal was formerly published in two sections: Section A "Physics and Chemistry" and Section B "Mathematical Sciences."

**DIMENSIONS/NBS**

This monthly magazine is published to inform scientists, engineers, businessmen, industry, teachers, students, and consumers of the latest advances in science and technology, with primary emphasis on the work at NBS. The magazine highlights and reviews such issues as energy research, fire protection, building technology, metric conversion, pollution abatement, health and safety, and consumer product performance. In addition, it reports the results of Bureau programs in measurement standards and techniques, properties of matter and materials, engineering standards and services, instrumentation, and automatic data processing.

Annual subscription: Domestic, $11.00; Foreign $13.75

## NONPERIODICALS

**Monographs**—Major contributions to the technical literature on various subjects related to the Bureau's scientific and technical activities.

**Handbooks**—Recommended codes of engineering and industrial practice (including safety codes) developed in cooperation with interested industries, professional organizations, and regulatory bodies.

**Special Publications**—Include proceedings of conferences sponsored by NBS, NBS annual reports, and other special publications appropriate to this grouping such as wall charts, pocket cards, and bibliographies.

**Applied Mathematics Series**—Mathematical tables, manuals, and studies of special interest to physicists, engineers, chemists, biologists, mathematicians, computer programmers, and others engaged in scientific and technical work.

**National Standard Reference Data Series**—Provides quantitative data on the physical and chemical properties of materials, compiled from the world's literature and critically evaluated. Developed under a world-wide program coordinated by NBS. Program under authority of National Standard Data Act (Public Law 90-396).

NOTE: At present the principal publication outlet for these data is the Journal of Physical and Chemical Reference Data (JPCRD) published quarterly for NBS by the American Chemical Society (ACS) and the American Institute of Physics (AIP). Subscriptions, reprints, and supplements available from ACS, 1155 Sixteenth St. N.W., Wash., D.C. 20056.

**Building Science Series**—Disseminates technical information developed at the Bureau on building materials, components, systems, and whole structures. The series presents research results, test methods, and performance criteria related to the structural and environmental functions and the durability and safety characteristics of building elements and systems.

**Technical Notes**—Studies or reports which are complete in themselves but restrictive in their treatment of a subject. Analogous to monographs but not so comprehensive in scope or definitive in treatment of the subject area. Often serve as a vehicle for final reports of work performed at NBS under the sponsorship of other government agencies.

**Voluntary Product Standards**—Developed under procedures published by the Department of Commerce in Part 10, Title 15, of the Code of Federal Regulations. The purpose of the standards is to establish nationally recognized requirements for products, and to provide all concerned interests with a basis for common understanding of the characteristics of the products. NBS administers this program as a supplement to the activities of the private sector standardizing organizations.

**Consumer Information Series**—Practical information, based on NBS research and experience, covering areas of interest to the consumer. Easily understandable language and illustrations provide useful background knowledge for shopping in today's technological marketplace.

*Order* **above** *NBS publications from: Superintendent of Documents, Government Printing Office, Washington, D.C. 20402.*

*Order* **following** *NBS publications—NBSIR's and FIPS from the National Technical Information Services, Springfield, Va. 22161.*

**Federal Information Processing Standards Publications (FIPS PUB)**—Publications in this series collectively constitute the Federal Information Processing Standards Register. Register serves as the official source of information in the Federal Government regarding standards issued by NBS pursuant to the Federal Property and Administrative Services Act of 1949 as amended, Public Law 89-306 (79 Stat. 1127), and as implemented by Executive Order 11717 (38 FR 12315, dated May 11, 1973) and Part 6 of Title 15 CFR (Code of Federal Regulations).

**NBS Interagency Reports (NBSIR)**—A special series of interim or final reports on work performed by NBS for outside sponsors (both government and non-government). In general, initial distribution is handled by the sponsor; public distribution is by the National Technical Information Services (Springfield, Va. 22161) in paper copy or microfiche form.

# BIBLIOGRAPHIC SUBSCRIPTION SERVICES

**The following current-awareness and literature-survey bibliographies are issued periodically by the Bureau:**

**Cryogenic Data Center Current Awareness Service.** A literature survey issued biweekly. Annual subscription: Domestic, $25.00; Foreign, $30.00.

**Liquified Natural Gas.** A literature survey issued quarterly. Annual subscription: $20.00.

**Superconducting Devices and Materials.** A literature survey issued quarterly. Annual subscription: $30.00. Send subscription orders and remittances for the preceding bibliographic services to National Bureau of Standards, Cryogenic Data Center (275.02) Boulder, Colorado 80302.

**U.S. DEPARTMENT OF COMMERCE**
**National Bureau of Standards**
Washington, D.C. 20234

OFFICIAL BUSINESS

Penalty for Private Use, $300

POSTAGE AND FEES PAID
U.S. DEPARTMENT OF COMMERCE
COM-215

SPECIAL FOURTH-CLASS RATE
BOOK